Hindawi
Geofluids
Volume 2019, Article ID 9545723, 23 pages
https://doi.org/10.1155/2019/9545723

Research Article

Preliminary Numerical Modeling of CO_2 Geological Storage in the Huangcaoxia Gas Reservoir in the Eastern Sichuan Basin, China

Hongwu Lei, Qian Zhang, and Xiaochun Li

State Key Laboratory of Geomechanics and Geotechnical Engineering, Institute of Rock and Soil Mechanics, Chinese Academy of Sciences, Wuhan 430071, China

Correspondence should be addressed to Hongwu Lei; hongwulei2008@aliyun.com

Received 17 June 2019; Revised 14 October 2019; Accepted 29 October 2019; Published 27 November 2019

Academic Editor: Paola Cianfarra

Depleted gas reservoirs are important potential sites for CO_2 geological sequestration due to their proven integrity and safety, well-known geological characteristics, and existing infrastructures and wells built for natural gas production. The Sichuan Basin has a large number of gas fields in which approximately 5.89×10^9 tons of CO_2 can be stored. The Huangcaoxia gas field has the best opportunity in the eastern Sichuan Basin for a pilot project of CO_2 sequestration due to its relatively large storage capacity and the nearly depleted state. A coupled thermal-hydrodynamic model including faults is built based on the geological and hydrogeological conditions in the Huangcaoxia gas field. The results of the numerical simulations show that the downhole temperature is above 80°C at a downhole pressure of 14 MPa under the constraint of temperature drop in the reservoir due to the strong Joule-Thomson effect. The corresponding injection pressure and temperature at the wellhead are 10.5 MPa and 60°C, respectively. The sizes of the pressure and CO_2 plumes after an injection of 10 years are 18 km and 5 km, respectively. The zone affected by temperature change is very small, being about 1-2 km away from the injection well. The injection rate in the injection well Cao 31 averages 6.89 kg/s (21.73×10^4 tons/a). For a commercial-scale injection, another four wells (Cao 9, Cao 30, Cao 6, and Cao 22) can be combined with the Cao 31 well for injection, approaching an injection rate of 35 kg/s (1.10×10^6 tons/a). Both the pressure and temperature of CO_2 injection decrease with the increasing depleted pressure in the gas reservoir when the latter is below 6 MPa. With the technique of CO_2-enhanced gas recovery (CO_2-EGR), the CO_2 injection rate is improved and approximately 1.58×10^7 kg of gas can be produced during a studied time period of 10 years.

1. Introduction

1.1. Background. CO_2 capture and storage is regarded as a technology of the highest potential for reducing CO_2 emissions from the combustion of fossil fuels in the short term [1]. Deep saline aquifers are considered to be the most promising sites for storing CO_2 due to their large storage capacity and wide distribution. However, the application of CCS in deep saline aquifers is hindered by some uncertainties and challenges, such as significant variation of storage capacity, limited information on geological characteristics, high costs associated with infrastructure construction, and the risk of CO_2 and brine leakage [2]. Depleted gas reservoirs are regarded as alternative candidates for CO_2 storage due to the integrity and safety proved by the accumulation and entrapment of natural gas, known geological characteristics from past natural gas production, and the fact that the preexisting in situ infrastructure and wells may be reused for CO_2 transport and injection [3]. The IEA (International Energy Agency) has estimated that, theoretically, up to 1300 Gt CO_2 could be sequestered in depleted gas reservoirs worldwide [4].

CO_2 storage in gas reservoirs can be classified into two types depending on its purpose. One type involves enhanced gas recovery (EGR) in partly depleted gas reservoirs by the mechanism of CO_2 displacement. CO_2 and CH_4 are, however, generally miscible with any proportion of both resulting in the risk of early CO_2 breakthrough in the production well and potential for requiring postrecovery separation of CO_2 from natural gas. The storage capacity of CO_2 associated with CO_2-EGR is limited because of the small density of CO_2

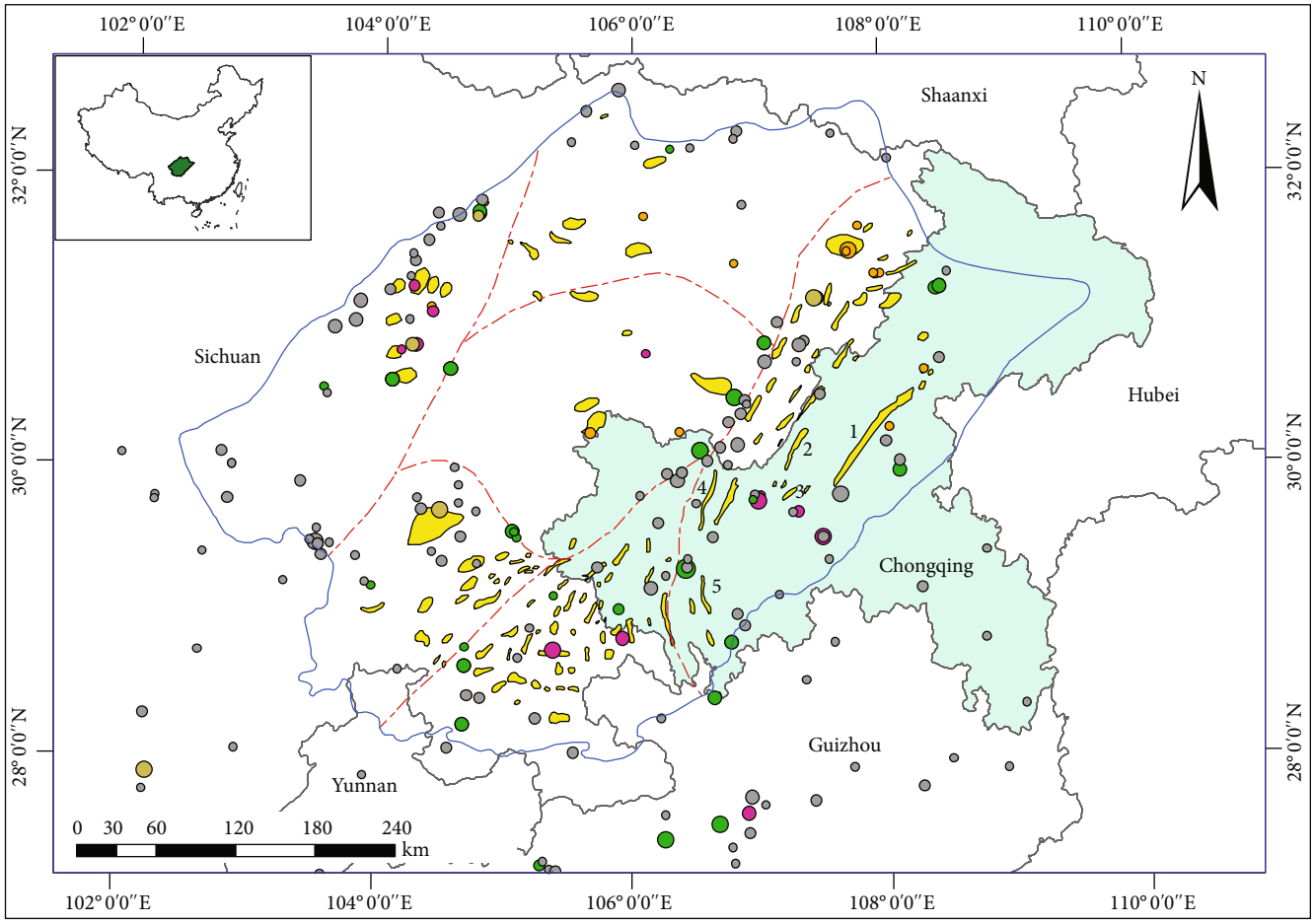

Note: 1. Dachigan gas field; 2. Wolonghe gas field; 3. Huangcaoxia gas field; 4. Xiangguosi gas field; 5. Shiyougou gas field

Legend

- Basin boundary
- Tectonic unit boundaries
- Gas field
- Cement plant
- Chemical plant
- Natural gas purification plant
- Power plant
- Steel plant

CO_2 emission (Mt/a)

- 0-0.5
- 0.5-1.0
- 1.0-2.5
- 2.5-5.0
- 5.0-6.0

Figure 1: Distribution of gas fields and CO_2 emission sources in the Sichuan Basin. Note: 1: Dachigan gas field; 2: Wolonghe gas field; 3: Huangcaoxia gas field; 4: Xiangguosi gas field; 5: Shiyougou gas field.

Table 1: Site characteristics of CO_2 storage in gas fields in the eastern Sichuan Basin.

Gas field	Dachigan	Wolonghe	Huangcaoxia	Shiyougou
CO_2 storage capacity (Mt)	65.55	51.7	22.9	7.39
Degree of exploitation	43% and 13 depleted wells	60% and 21 depleted wells	90% and 11 depleted wells	77% and 4 depleted wells
Number of CO_2 emission sources within 50 km	10	14	11	11
Total amount of CO_2 emission within 50 km (Mt/a)	14.26	24.04	22.81	17.50
Type[a] of CO_2 emission within 50 km	1, 2, 3	1, 2, 3, 4	1, 2, 3, 4	1, 3
Site screening	—	Option	Best	—

[a]1: cement plant; 2: chemical plant; 3: thermal power plant; 4: steel plant.

especially at low average pressure in the reservoir. The other type is strictly for storing CO_2 when the gas reservoir is depleted or CO_2-EGR is completed.

There are a few pilot projects testing the feasibility of CO_2 storage in depleted gas reservoirs: the K12-B CO_2 Injection Project in the Netherlands, the Lacq CCS Pilot Project in

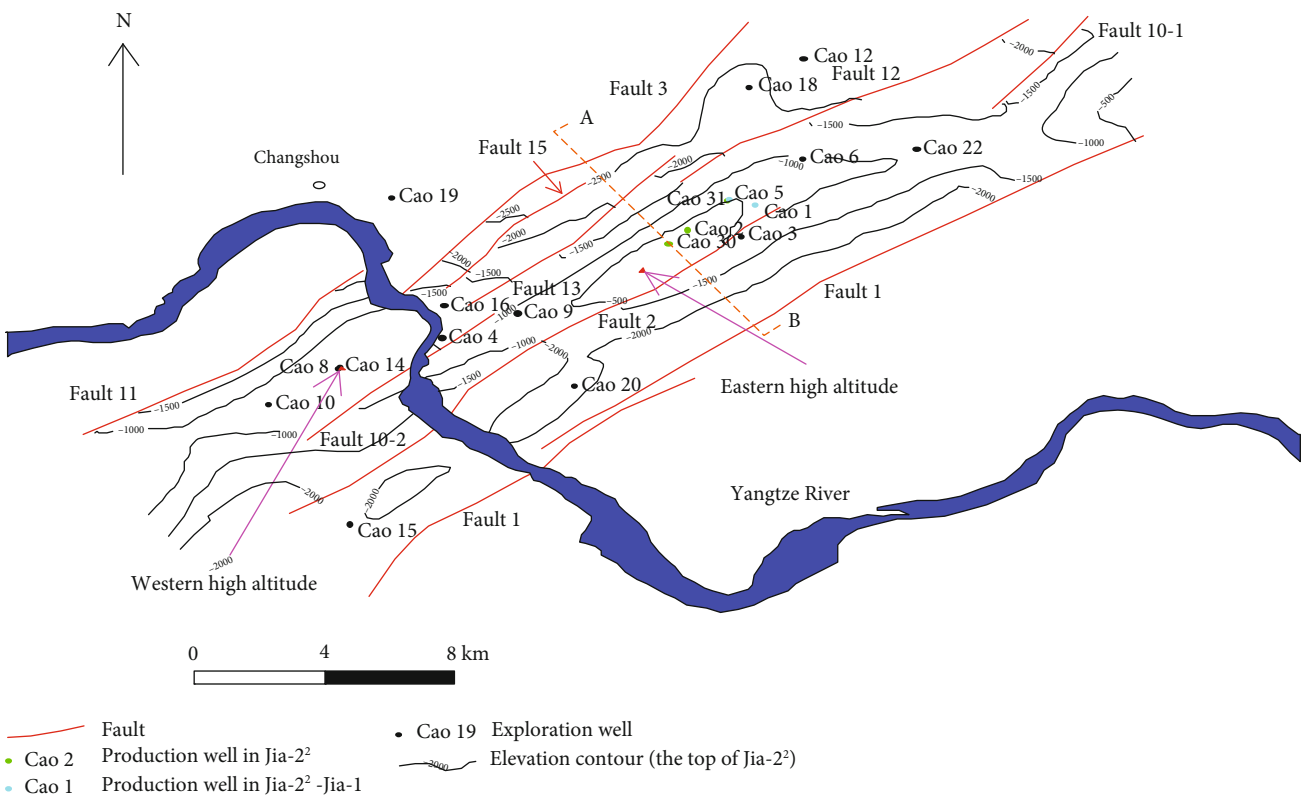

(a)

Strata			Bottom depth (m)	Lithological properties	Gas layer	For CO_2 storage	
System	Formation	Layer				Reservoir	Caprock
Triassic	Jianlingjiang	Jia-5	423	Dolomite and calcite,interbed gypsum			
		Jia-4	840	Gypsum in the middle and top,calcite at the bottom			
		Jia-3	909	Calcite			
		Jia-2	1036	Jia-2¹: gypsum,dolomite,calcite,gypsum Jia-2²: dolomite and gypsum Jia-2¹: gypsum			
		Jia-1	1254	Calcite			

Dolomite
Calcite
Gpysum

(b)

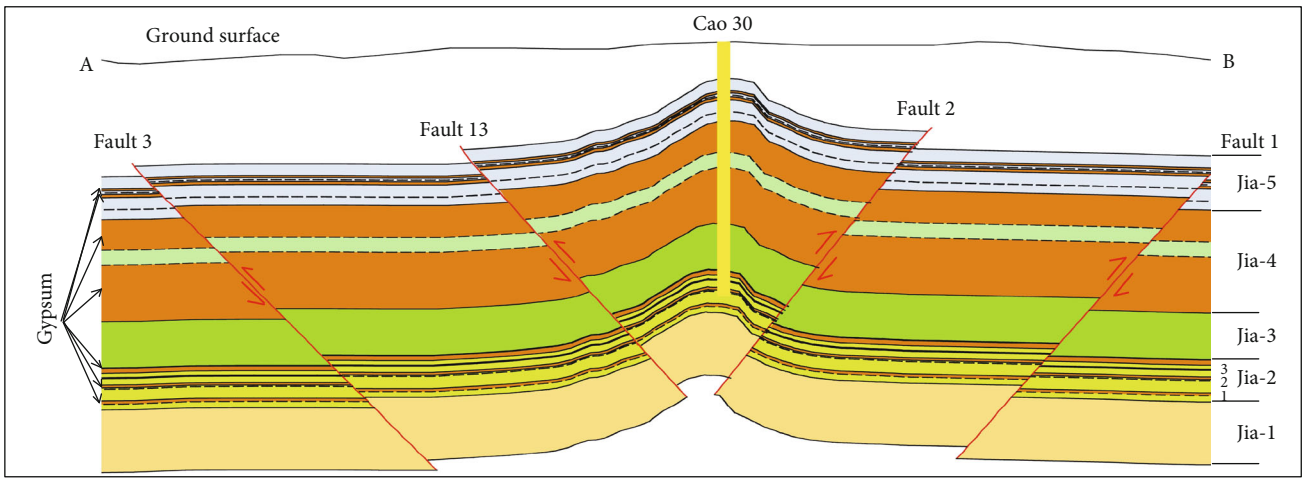

(c)

Figure 2: Structure map of the top boundary of Jia-2² reservoir (a), stratigraphic column of Jialingjiang formation (b), and profile of the gas reservoir (c).

Table 2: Hydrogeological properties of the reservoir.

Reservoir	R_f	OGIP (10^8 m^3)	P_s (MPa)	T_s (°C)	Z_s	P_r (MPa)	T_r (°C)	Z_r	$\rho_{CO_2 res}$ (kg/m^3)	M_{CO_2} (10^4 ton)
Jia-2^1/Jia-1	0.9	20.93	0.101	20	0.998	14.12	43	0.843	698.7	860
Jia-2^2	0.9	33.84	0.101	20	0.998	13.83	40	0.834	720.3	1430
Total						2290				

Note: the CO_2 storage capacity is calculated by $M_{CO_2} = \rho_{CO_2 res} R_f (1 - F_{IG}) \bullet \text{OGIP} \bullet [(P_s Z_r T_r)/(P_r Z_s T_s)]$ [23], where $\rho_{CO_2 res}$ is the density of CO_2 at the reservoir conditions. R_f is the recovery factor and set to be 0.9. F_{IG} is the fraction of injected gas and equal to 0. P, T, and Z are the pressure, temperature, and gas compressibility factor, respectively. The subscripts r and s denote, in this order, the reservoir and surface conditions. The values of the parameters contained in Table 2 are calculated from GasEOS (http://esdtools.lbl.gov/gaseos/ [24]).

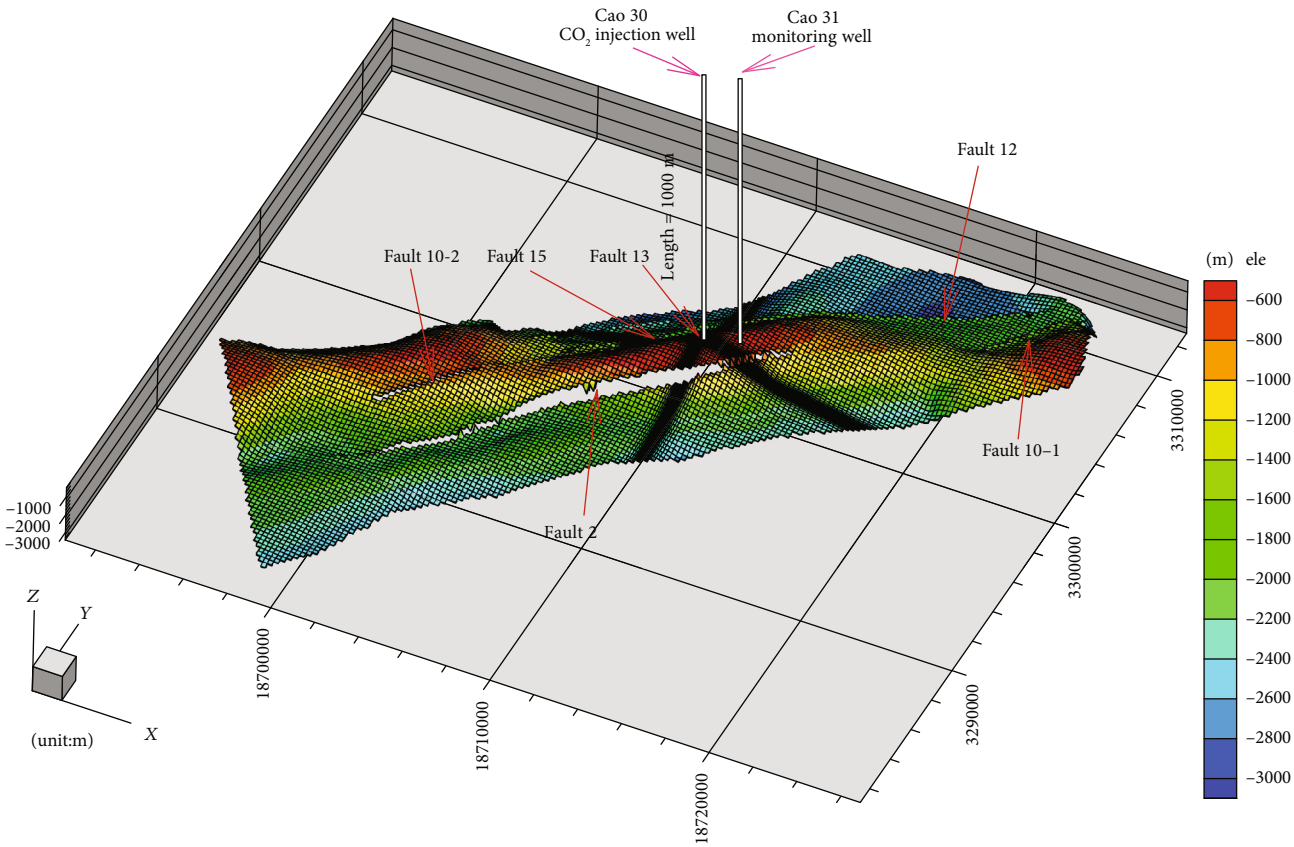

Figure 3: Grid discretization for the Jia-2^2 formation.

France, the CLEAN Project in Germany, and the CO2CRC Otway Project in Australia. The K12-B project is dedicated to determine the potential for both CO_2 storage and EGR. The gas reservoir is at the depth of about 3800 m with initial pressure of 40 MPa and temperature of 127°C [5]. Pressure has dropped to about 40 bar at the beginning of CO_2 injection. A total of 90,000 tonnes of CO_2 has been injected at the downhole pressure of about 100 bar and temperature of 120°C. The first French CO_2 capture and storage pilot conducted by TOTAL is to demonstrate the technical feasibility and reliability of an integrated CO_2 capture, transportation, injection, and storage into a depleted gas field. The rich CO_2 stream from an oxygen-gas combustion boiler is transported as a gas phase via existing pipelines to the Rousse gas field which is at a depth of 4500 m and was depleted to a 4 MPa in 2008 [6]. A total of 45,000 tonnes of CO_2 has been injected from 2010 to 2013, and two and a half years of monitoring during the injection have demonstrated that the CO_2 remains well confined within the reservoir [7]. The CLEAN project conducted in the years 2008-2011 was to investigate the processes relevant to EGR by the injection of CO_2 into a subfield of the almost depleted Altmark natural gas field. Despite the setback that permission for CO_2 injection was not issued by the mining authority, the results from a comprehensive evaluation provided the technological, logistic, and conceptual prerequisites for implementing a CO_2-based EGR project [8]. The CO2CRC Otway Project is one of the most successful demonstrated projects for CO_2 storage in depleted gas reservoirs. A total of 65,445 tonnes of CO_2-rich mixed gas (75.4 mol% CO_2 and 20.5 mol% CH_4 in average) from a nearby gas field was injected at an average rate of about 870 tonnes per week into the water leg of the Naylor

gas field with an estimated CO_2 storage capacity of 113,000 to 115,000 tonnes [9]. The target reservoir is at the depth of about 2000 m, and the pressure is 11 MPa at the beginning of CO_2 injection (decreased from initial pressure of 19.59 MPa to 11 MPa due to gas production) [9]. The monitoring results, from water and gas samples at the potable aquifers and vadose zones, U-tube fluid sampling apparatus in the reservoir, and seismic surveying confirm that CO_2 storage in depleted gas fields can be safe and effective [10]. These projects can provide experience for China to implement the first CO_2 injection into a depleted gas reservoir in the Sichuan Basin.

CO_2 injection into a depleted gas reservoir involves multiphase and multicomponent transport and sometimes heat convection and thermal conduction. Numerical simulation offers an effective tool for quantifying these processes. Oldenburg et al. [11, 12] simulated the process of injecting CO_2 into the Rio Vista Gas Field using TOUGH2/EOS7C [13] and showed that carbon sequestration with enhanced gas recovery (CSEGR) allows more than five times of CH_4 recovery than otherwise and that the economic feasibility of CSEGR was most sensitive to wellhead methane price, CO_2 supply costs, and the ratio of CO_2 injection cost to the increments of methane price. Ennis-King et al. [14] performed history matching of simulation to field data for the CO2CRC Otway Project with TOUGH2/EOS7C and showed that the key features of the field data including the downhole pressure and the arrival time at the observation well can be captured by numerical simulations, which increased the confidence in the feasibility of CO_2 storage in depleted gas reservoirs. A dynamic model based on GEM was built to simulate the migration of CO_2 in the reservoir for the Lacq CCS Pilot Project and its contact with the caprock, the water vaporization around the injector, and associated risk of salt plugging, as well as the change of pH value in the reservoir [15]. Gou et al. [16] developed a coupled hydromechanical simulator TOUGH2MP/EOS7C-FLAC3D for modeling the pressure buildup, the CO_2 migration, and the uplift of ground surface in different scenarios of CO_2 injection and gas production for the CLEAN Project. Oldenburg [17] evaluated the change of temperature in a natural gas reservoir after the injection of CO_2 due to the Joule-Thomson effect using TOUGH2/-EOS7C and showed that the reservoir temperature could be reduced by 20°C in the case of high-pressure injection into a reservoir at low pressure. Luo et al. [18] built an optimized model to study the effects of vertical permeability heterogeneity and the depth of perforation in injection/production wells on the CSEGR performance using the software FLUENT. Recently, Patel et al. [19] used COMSOL to simulate the CO2-EGR taking into consideration the tortuosity of the flow path in the reservoir rock and the dispersivity which have significant effects on the CH_4-CO_2 mixing process.

1.2. Potential Gas Fields for CO_2 Storage in the Eastern Sichuan Basin. The Sichuan Basin with an area of about 230,000 km^2 in southwest China is one of the four largest basins in China. The Sichuan Basin represents one of China's largest natural gas-bearing basins with 125 gas fields found in the Jurassic, Triassic, Permian, Carboniferous, and Upper Proterozoic strata. The accumulated discovered natural gas is about $17{,}225 \times 10^8$ m^3 [20]. Behind the Ordos Basin with the highest CO_2 storage potential, the Sichuan Basin has the second highest potential basin for CO_2 storage in depleted gas reservoirs, with the capacity of 5.89×10^9 tons [21].

Table 3: Hydrogeological properties of the reservoir.

Parameters	Values
Thickness	20 m
Permeability	7.0 mD
Porosity	0.05
Compressibility	4.5×10^{-10} Pa^{-1}
Temperature	40°C
Salinity	0.067
Injection well	Cao 30 (radial of 0.09 m, depth of 1000 m)
Monitoring well	Cao 31
Relative permeability model:	
Liquid [29]	
$k_{rl} = \sqrt{S^*}\left\{1 - \left(1 - [S^*]^{1/m}\right)^m\right\}^2$	$S^* = S_l - S_{lr}/1 - S_{lr}$
S_{lr}: residual water saturation	$S_{lr} = 0.15$
m: exponent	$m = 0.457$
Gas [30]:	
$k_{rg} = (1 - S\wedge)^2\left(1 - S\wedge^2\right)$	$\widehat{S} = S_l - S_{lr}/S_l - S_{lr} - S_{gr}$
S_{gr}: residual gas saturation	$S_{gr} = 0.05$
Capillary pressure model [29]:	
$P_{cap} = -P_0\left([S^*]^{-1/m} - 1\right)^{1-m}$	$S^* = S_l - S_{lr}/1 - S_{lr}$
S_{lr}: residual water saturation	$S_{lr} = 0.05$
m: exponent	$m = 0.457$
P_0: strength coefficient	$P_0 = 19,350$ Pa

Based on the previous preliminary evaluation considering the CO_2 storage capacity (>10 million tons) and gas production status (nearly depleted), there are four potential gas fields for CO_2 storage in depleted gas reservoirs in the eastern Sichuan Basin: Dachigan, Wolonghe, Huangcaoxia, and Shiyougou [22] (Figure 1). Table 1 lists the main features of the four potential sites. The Shiyougou gas field is unsuitable for the ten million tons scale project because of its small storage capacity. The Dachigan and Wolonghe gas fields both have a capacity of over 50 million tons for CO_2 storage and have good source-sink matching. Although these two gas fields are in the last stage of exploitation, they could not be completely depleted in the short term. They can be used as alternative sites for CO_2 storage in the medium-long term. Although the Huangcaoxia gas field has a relatively small storage capacity, it is currently at the end stage of exploitation and will be depleted completely in the next 2 or 3 years. Therefore, the Huangcaoxia gas field is the best option to be the storage site for the demonstration project. The nearest CO_2 emission sources from the gas field are located in Yanjia industrial park within about only 20 kilometers in a straight line.

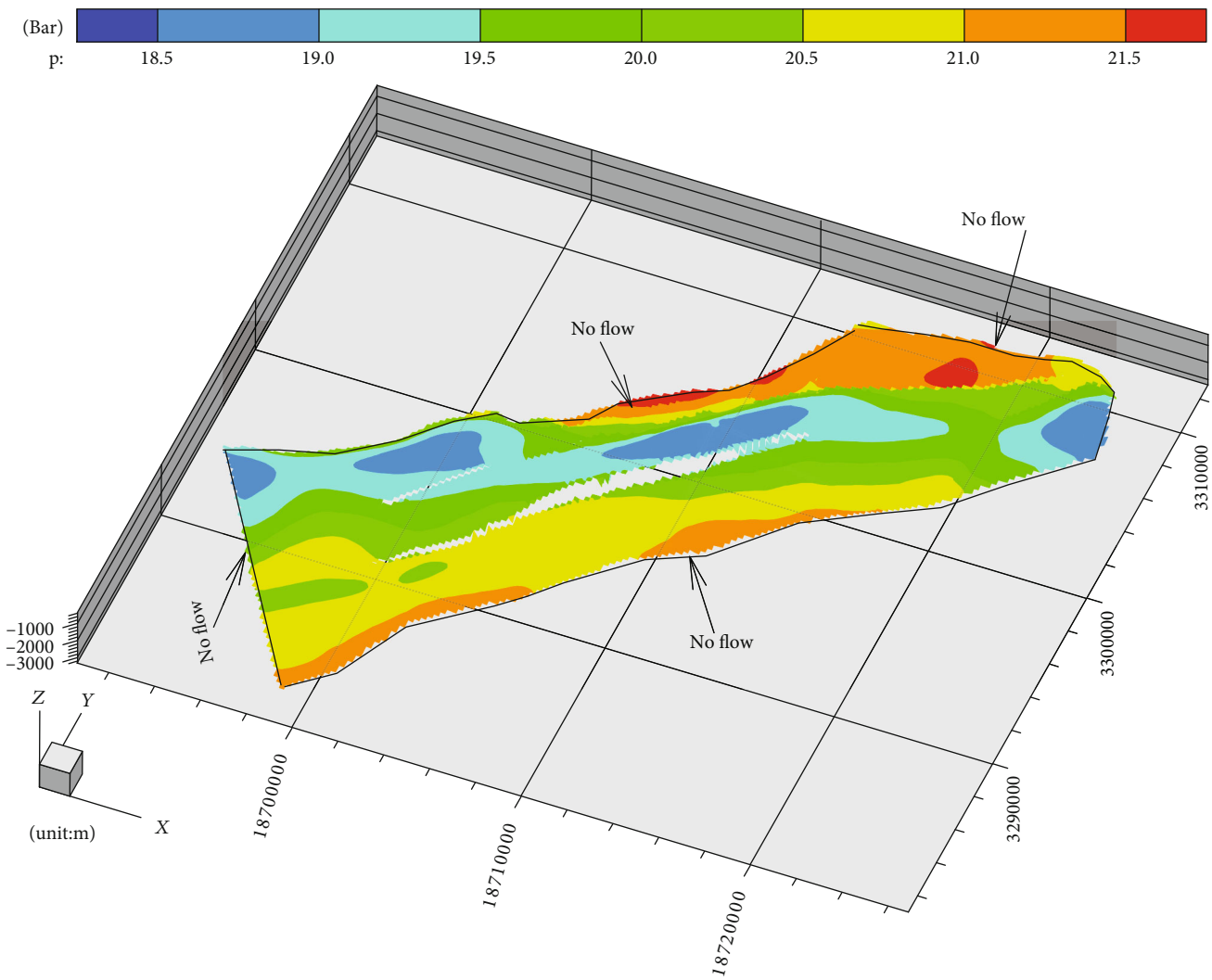

Figure 4: Distribution of initial pressure for Jia-2[2] reservoir.

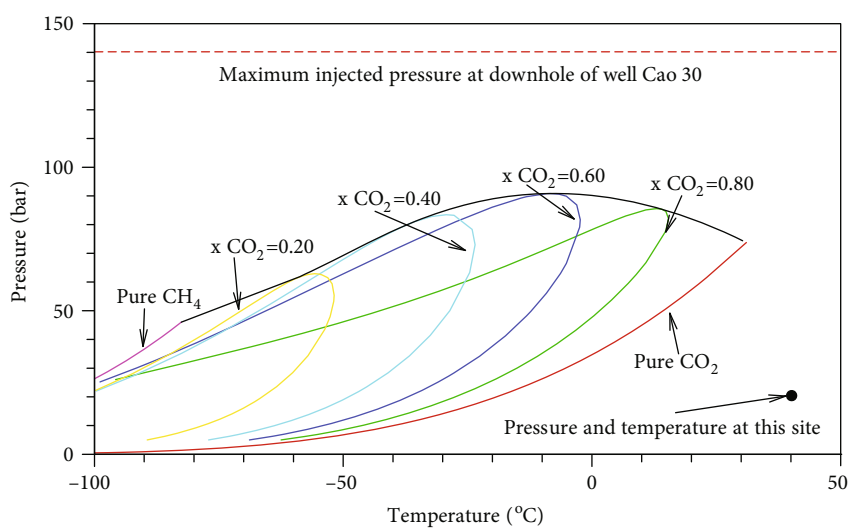

Figure 5: Phase envelope of CO_2-CH_4 systems, calculated by PVTSim [31].

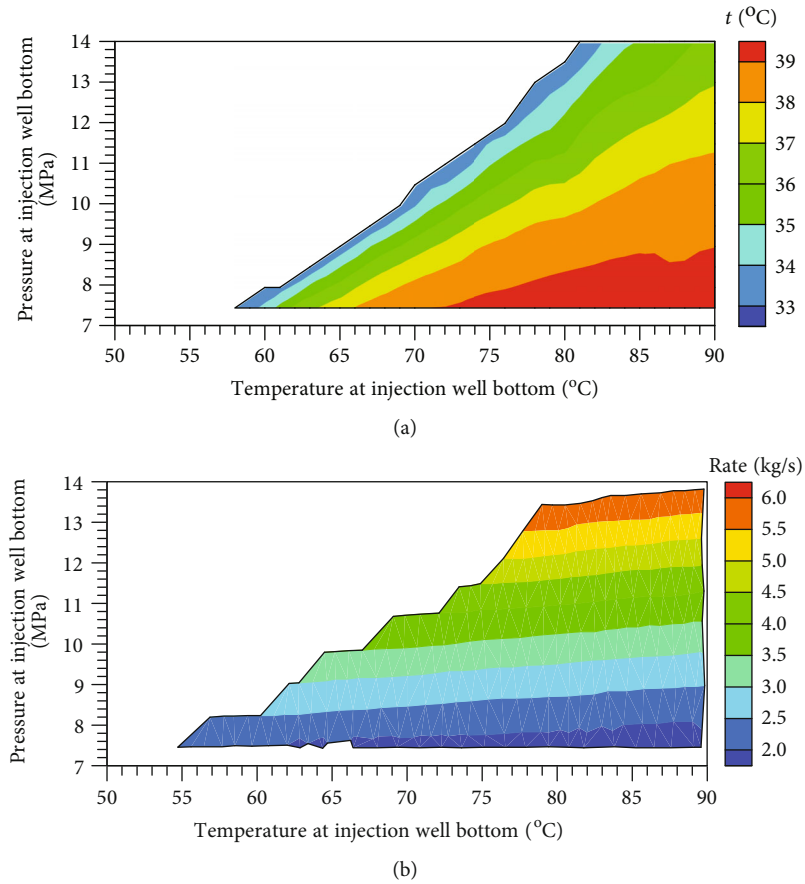

Figure 6: The experienced lowest temperature for the reservoir (a) and corresponding injection rate (b) with injection pressures and temperatures.

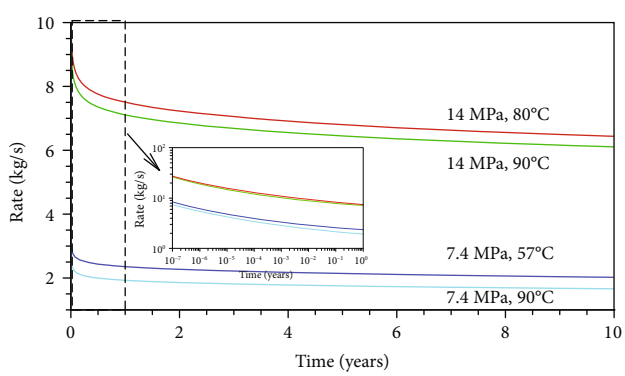

Figure 7: Variation of injection rate with time at the well Cao 30.

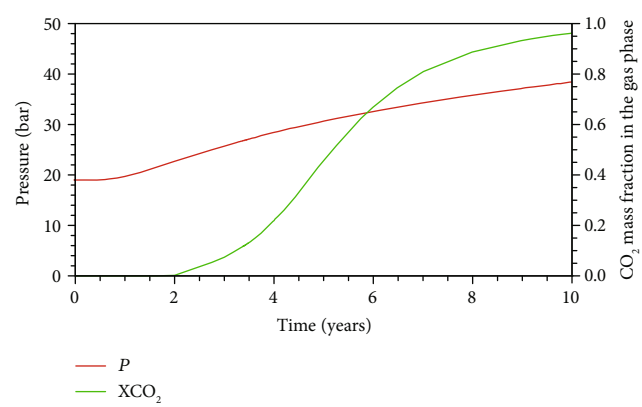

Figure 8: Variation of pressure and CO_2 mass fraction in the gas phase at the monitoring well Cao 31.

2. Geological Characteristics and CO_2 Storage Capacity in the Huangcaoxia Gas Field

2.1. Geological Characteristics. Huangcaoxia structure is a NE-trending anticline in which there are two structural high points along the eastern and western high altitudes, respectively (Figure 2(a)). The gas production strata are mainly located in the Lower Triassic Jialingjiang Formation (Jia-2^2 and Jia-2^1/Jia-1) (Figure 2(b)). The Jia-2^2 reservoir is at a depth of 1000 m and has thickness ranging from 21.50 to 25 m (Figure 2(c)). The reservoir is dominated by dolomite with embedded anhydrite. Natural gas in the Jia-2^2 reservoir is mainly composed of hydrocarbons (>97%) with minor contents of CO_2 (0.25~0.14 g/m^3) and H_2S (12.48~13.72 g/m^3). The initial pressure and the average reservoir temperature are 13.84 MPa and 40°C, respectively. The fractured Jia-2^1/Jia-1 reservoir which is composed of calcite with embedded anhydrite is located at a depth of 1160 m and has lower content of H_2S (0.30 g/m^3) compared with the Jia-2^2 reservoir. The initial pressure and the average reservoir temperature

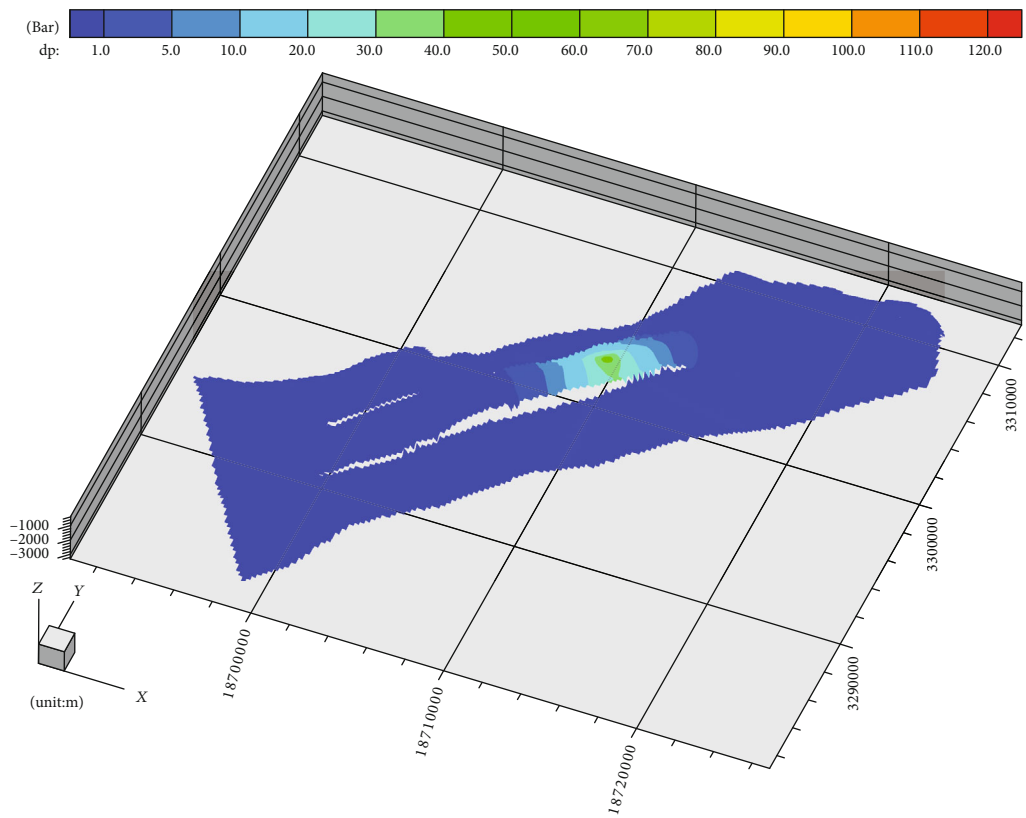

(a)

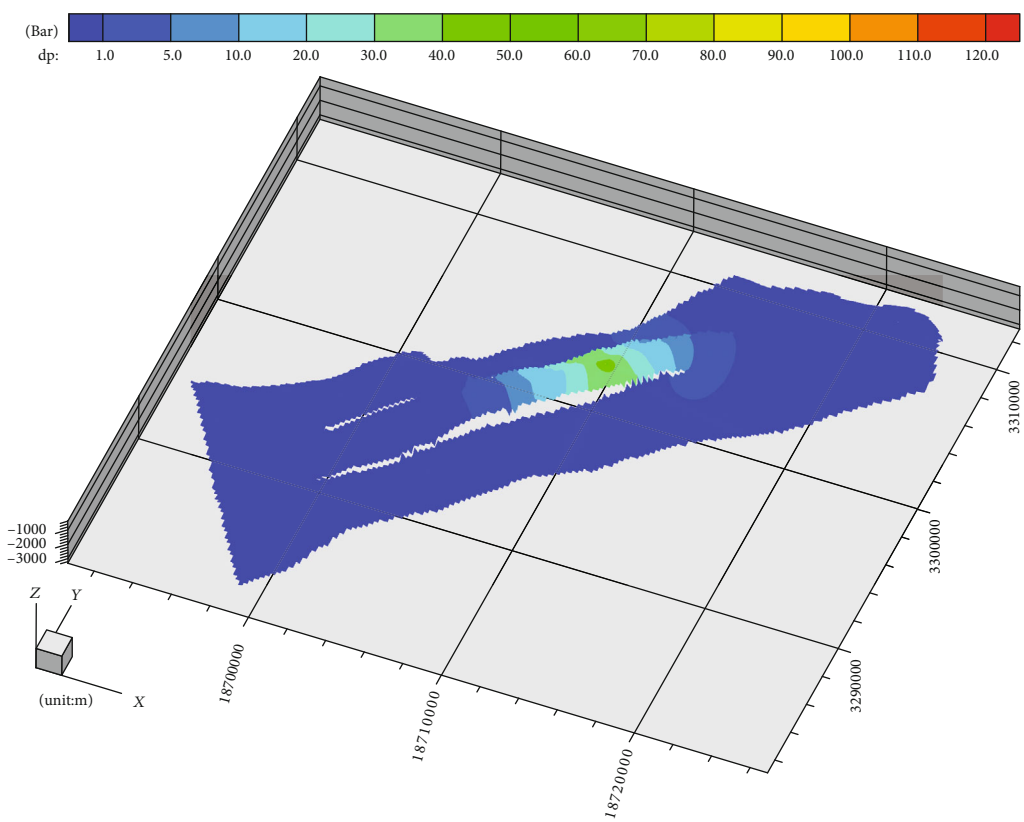

(b)

Figure 9: Continued.

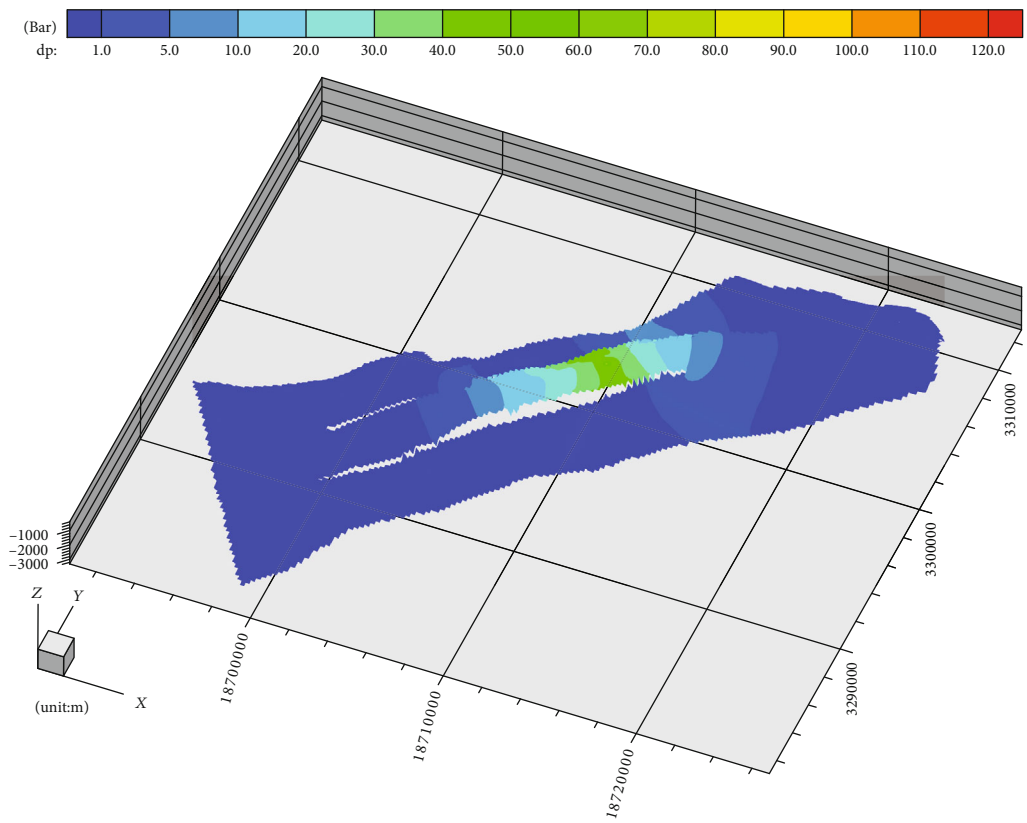

(c)

Figure 9: Spatial distribution of pressure increment after CO_2 injection over 3 years (a), 6 years (b), and 10 years (c).

are 14.12 MPa and 43°C, respectively. During the long-term gas production, the reservoir pressure has decreased to about 2 MPa.

2.2. CO_2 Storage Capacity. Following the evaluation method introduced by Bachu and Shaw [23] for CO_2 storage in depleted gas reservoirs, the CO_2 storage capacity in the Huangcaoxia gas field is estimated and listed in Table 2. Due to the highly evolved pore space and relative large storage capacity, the Jia-2^2 reservoir is considered to be the priority target for CO_2 injection.

3. Model Setup

3.1. Simulation Tool. TOUGH2 is widely used to simulate nonisothermal multiphase and multicomponent flow for CO_2 geological sequestration (e.g., [12, 25, 26]). EOS7C [13] is one of the TOUGH2 modules for simulating the direct injection of CO_2 into depleted natural gas (e.g., CH_4) reservoirs. This module handles CH_4-CO_2-brine or CH_4-N_2-brine systems at temperatures up to 110°C. Lei et al. [27, 28] extended TOUGH2/EOS7C to consider the effect of other gas components such as H_2S and O_2 as well as high-temperature conditions (up to 200°C). In the present study, we used the TOUGH2 module extended by Lei et al. (i.e., EOS7Cm) to simulate the coupled thermal-hydrodynamic process for CO_2 injection into the Huangcaoxia gas reservoir.

3.2. Geometry, Grid Discretization, and Parameters. According to the results of seismic exploration, the southeast and northwest boundaries of the Huangcaoxia structure are closed by the faults F1 and F3 (Figure 2(a)), respectively. The northeast and southwest boundaries are open. The area of the structure is approximately 300 km^2 with a length of about 36 km and a width of about 9 km. The average thickness of the main reservoir formation Jia-2^2 is 20 m. The reservoir is cut by the multiple sealing faults (i.e., F2, F10, F11, F12, F13, and F15).

In the simulation, CO_2 is only injected into the Jia-2^2 formation. Due to limited geology data, it is difficult to construct a read model (e.g., MINC model) to consider fractures in the model. As a result, the porous-fractured reservoir is characterized as porous media with no fractures in the model. However, it is worth noting that there are some differences between CO_2 storage or CO_2-EGR in a porous-fractured reservoir and in a porous reservoir with no fractures. The porous-fractured reservoirs may deplete with respect to pressure long before they deplete with respect to natural gas. The pressure in the fractures could rebound because the natural gas which is filled in the pore transfers from matrix rocks to fractures. This process can affect the CO_2 injection and transportation. Though our model does not consider the presence of fractures and thus has limitations, our model is able to provide useful results of pressure and CO_2 saturation distributions and can be used in the future as the basis for more detailed and site-specific modeling of the site.

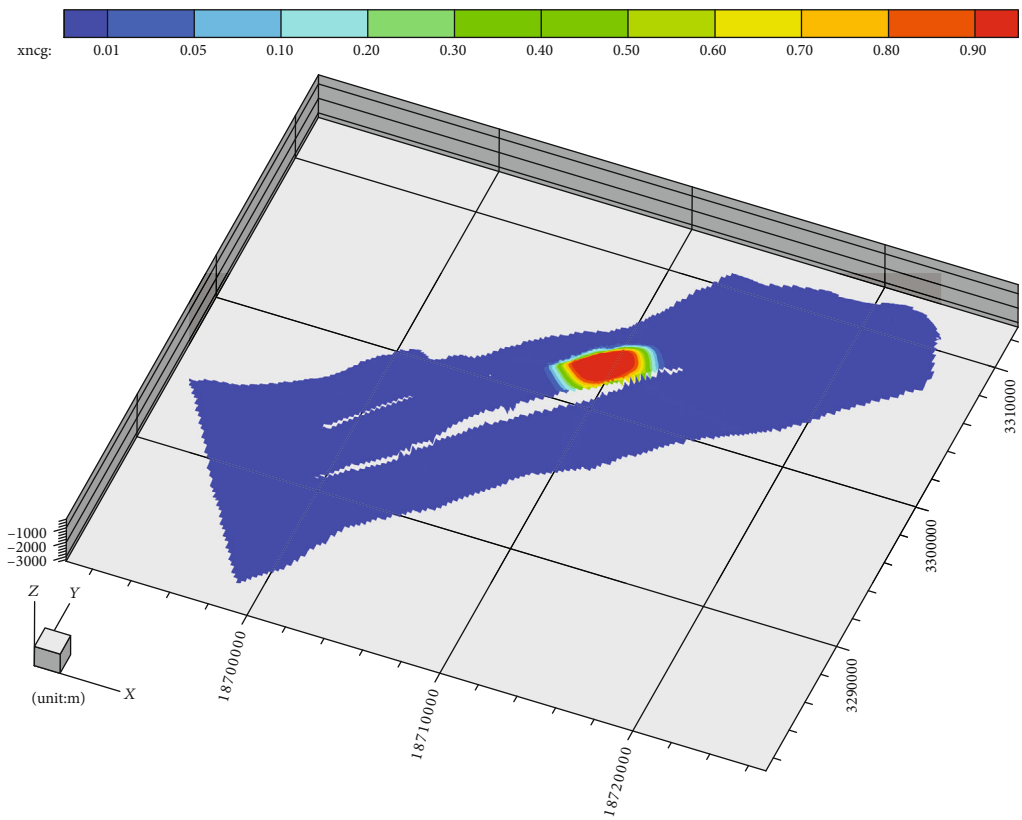

(a)

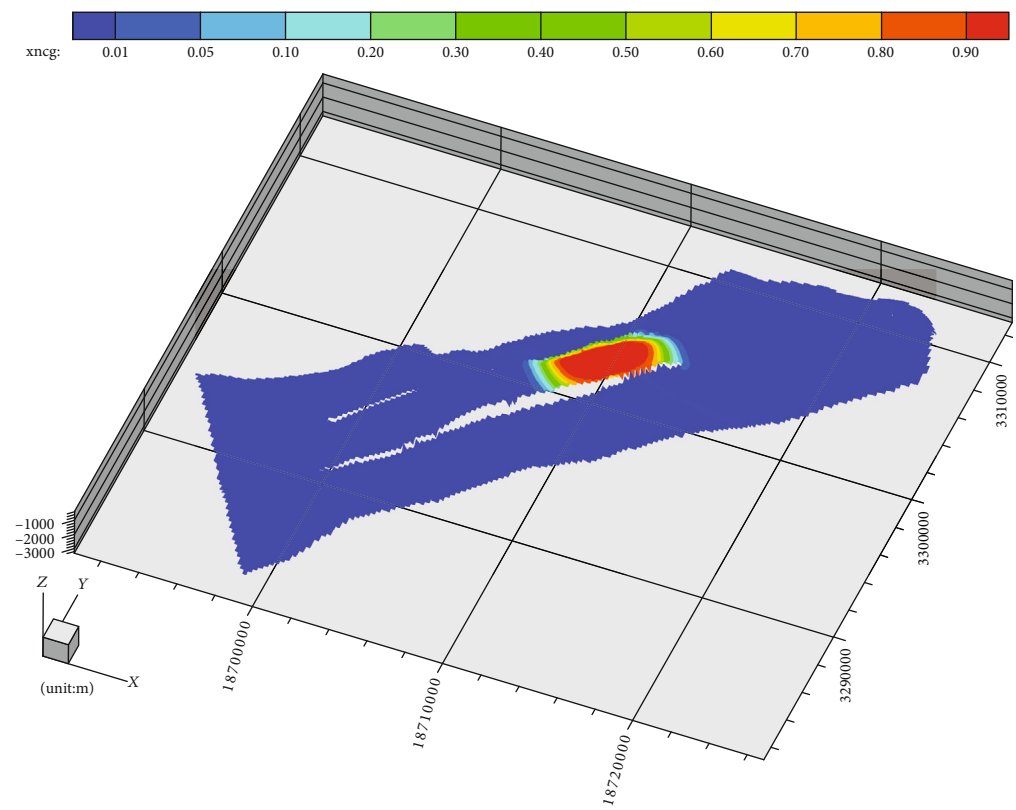

(b)

Figure 10: Continued.

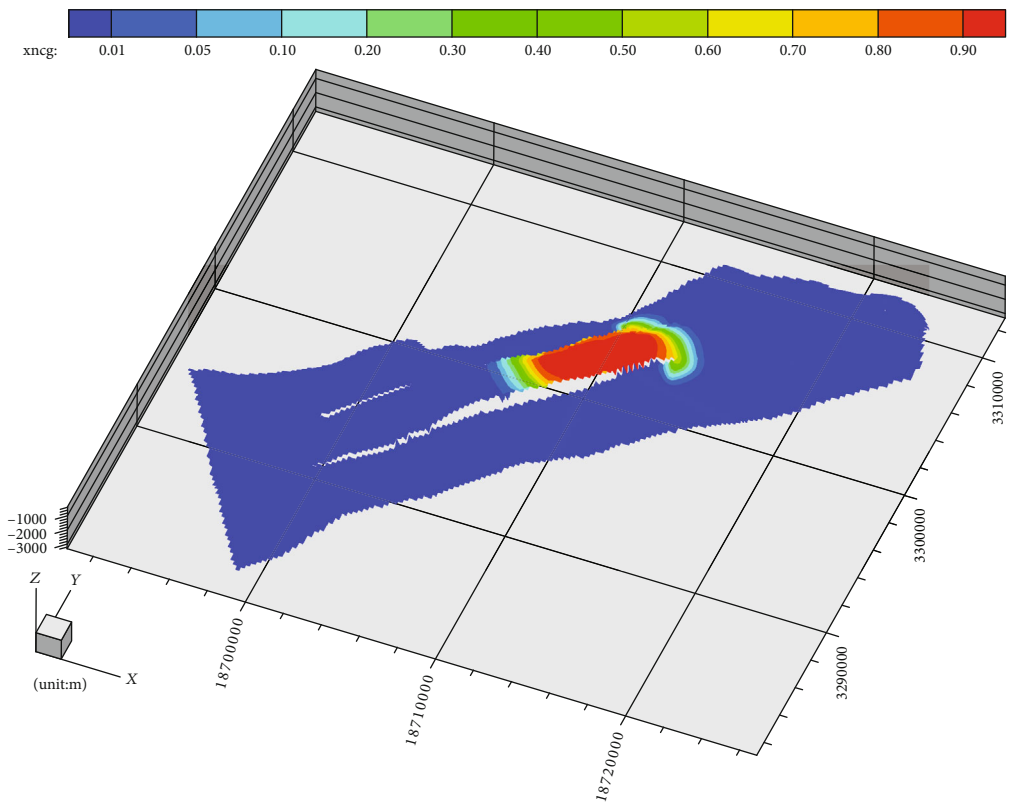

(c)

Figure 10: Spatial distribution of CO_2 mass fraction in the gas after CO_2 injection over 3 years (a), 6 years (b), and 10 years (c).

The injection well (Cao 30) is near the peak point in the northeast region, and the monitoring well (Cao 31) is 2600 m away from the injector. A regular Cartesian grid is employed to represent the reservoir. The grid blocks of varying sizes, from 0.09 m near the wells to 200 m in the far field, are set in order to capture the drastic change in pressure and temperature close to the well. In the vertical direction, only one layer is used. The faults are also included in the space discretization. The total number of valid grids is 19,389, consisting of 285 and 265 grid blocks in the X- and Y-directions, respectively. Figure 3 shows the result of grid discretization.

The model involves hydrogeological and geological parameters, such as thickness, permeability, porosity, relative permeability, and capillary pressure, which are listed in Table 3.

3.3. Initial and Boundary Condition. The Huangcaoxia gas field is nearly depleted, and the reservoir pressure decreases to about 2 MPa based on the measurement at the well Cao 30. It is assumed that the pressure distribution reaches equilibrium at a small production rate. In the model, a fixed pressure of 2 MPa is set for the grid in which the Cao 30 well is located and a long simulation time (100 years in the present study) is needed to obtain the initial pressure. Figure 4 shows that the distribution of pressure is controlled by the reservoir topography.

The lateral boundaries are all set to be no-flux, i.e., closed. It is noted that the geological features suggest that the southwestern and northeastern boundaries are close to open boundaries. However, it is difficult to determine the flux across the two boundaries, and the two boundaries are set as no-flux boundaries in the model. No-flux boundaries result in higher pressure buildup than open boundaries, and thus, the choice of no-flux boundaries for the southwestern and northeastern boundaries represents a worst-case scenario that allows maximum pressure buildup.

3.4. CO_2 Injection Strategy. To manage the pressure buildup, CO_2 is injected at a constant pressure. The upper limit of the downhole pressure is set to be equivalent to the initial reservoir pressure of 14 MPa prior to natural gas recovery in order to avoid damaging the reservoir. Meanwhile, the pressure in the injection well should be over the supercritical pressure of 7.4 MPa to improve the injectivity. The pressurized CO_2 injected into the depleted gas reservoir would induce a large reduction in temperature in the vicinity of the wellbore due to the strong Joule-Thomson effect, resulting in the possible phase change of fluids and damage in the wellbore and the reservoir. In order to avoid the potential thermally induced damage and to keep the single-phase mixture of CO_2 and CH_4 (Figure 5), the lowest experienced temperature in the reservoir should be higher than the critical temperature of 31.26°C. In order to meet the requirements raised by the aforementioned factors, the optimized downhole temperature is determined by simulation over an injection time period of 10 years.

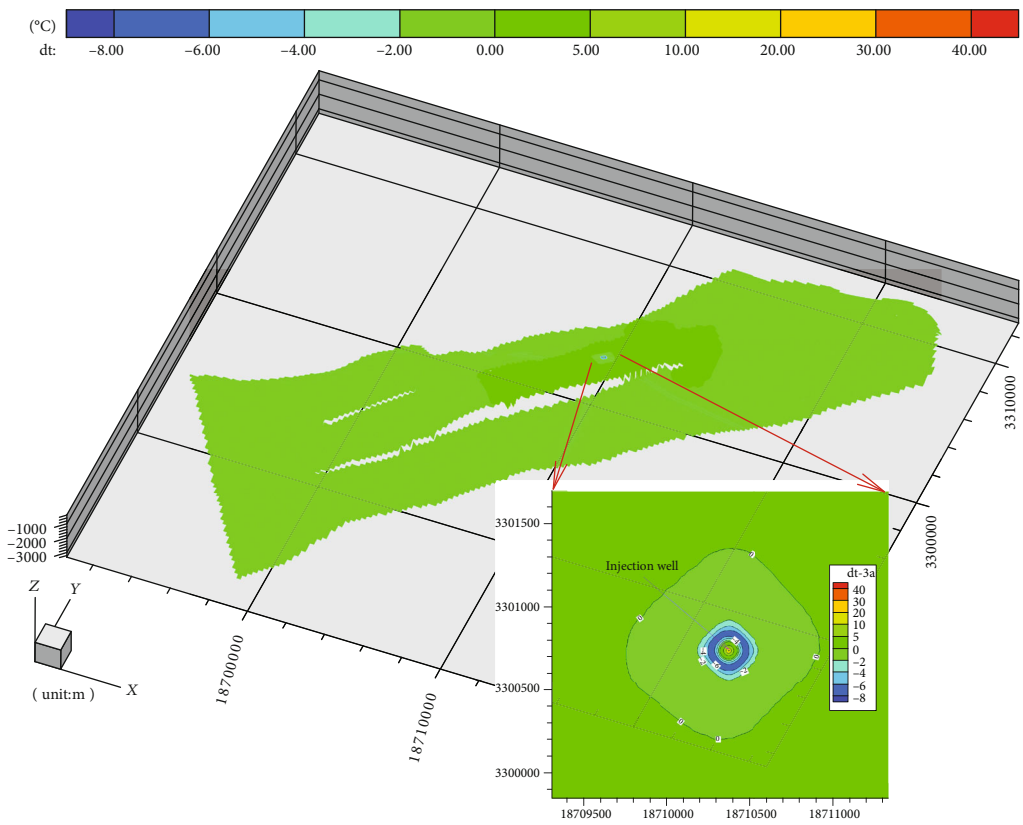

(a)

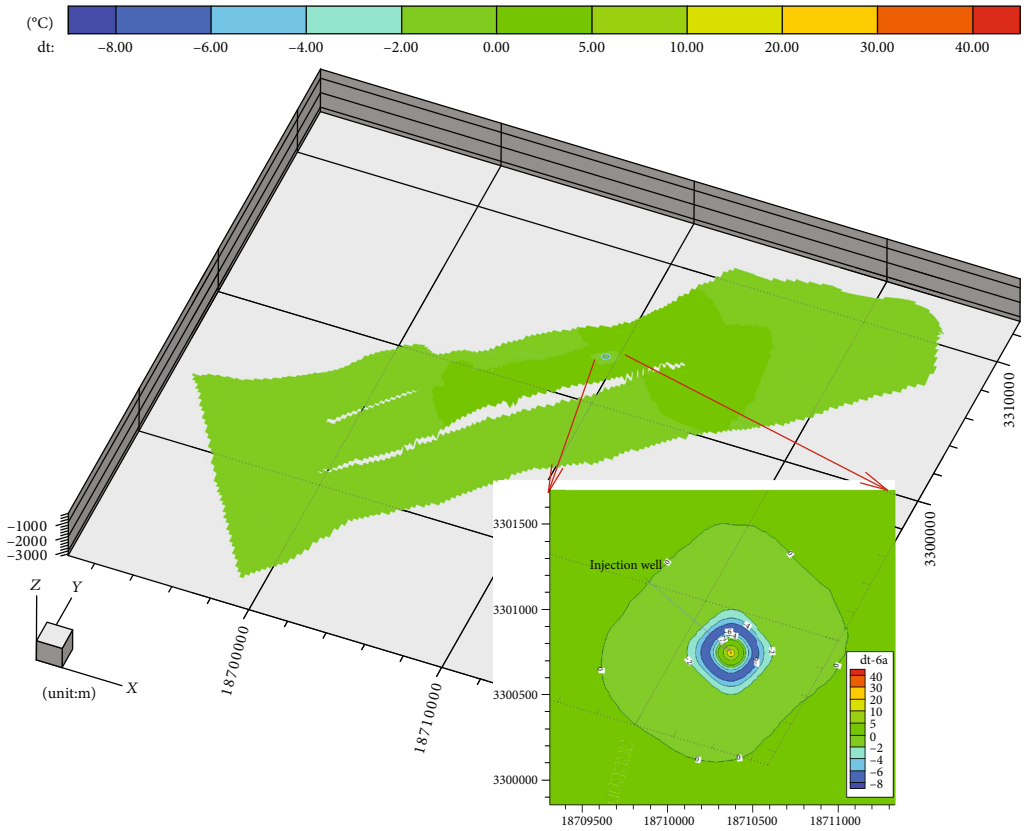

(b)

Figure 11: Continued.

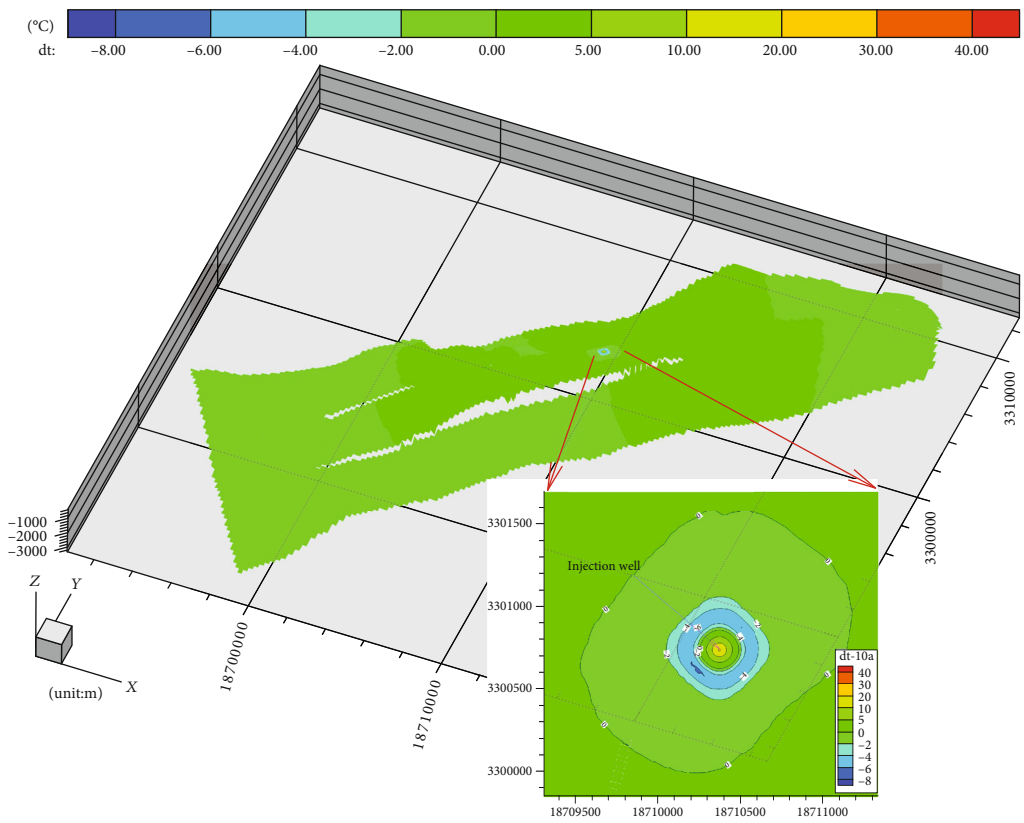

(c)

Figure 11: Spatial distribution of temperature increment after CO_2 injection over 3 years (a), 6 years (b), and 10 years (c).

4. Results

4.1. Reservoir. To analyze the influence of injection pressure on the injection temperature at the downhole and find the effective range of pressure and temperature for injection taking into account the controlling factors mentioned above, totally 160 combinations of pressures from 7.4 MPa to 14 MPa with an interval of 1 MPa and temperatures from 52°C to 90°C with an interval of 2°C are employed. Figure 6(a) shows that the required lowest downhole temperature is about 55°C and the higher the injection pressure, the higher the injection temperature should be. The injection rate ranges from 1.5 kg/s (4.5×10^4 tons/a) to 6.5 kg/s (20.4×10^4 tons/a) (Figure 6(b)), showing a stronger dependence on pressure than on temperature. To maximize the injection rate, a downhole pressure of 14 MPa and a downhole temperature of 80°C are suggested for CO_2 injection. The suggested values of the injection parameters are used hereinafter.

Figure 7 shows the injection rates under four typical injection conditions. At the downhole pressure of 14 MPa and the temperature of 80°C, the injection rate decreases gradually from 10.0 kg/s to 6.4 kg/s delivering an average of 6.89 kg/s (21.73×10^4 tons/a). At a fixed injection pressure, a high injection temperature does not contribute to increase of the injection rate as the density (ρ) and viscosity (μ) of the injectant tend to simultaneously decrease in the range of temperature above the critical temperature of 31.26°C and both of the parameters control the mobility (ρ/μ) as well as the mass flow rate of the injection. Also, the behavior of scCO2 viscosity decrease with temperature is different from that of gases, for which viscosity normally increases with temperature.

Figure 8 shows that injected CO_2 arrives at the monitoring well Cao 31 after an injection period of 2 years. The velocity of pressure diffusion [32] is faster than that of CO_2 transport. After an injection over 3 years, the pressure and CO_2 mass fraction in the gas phase at the monitoring well increase to 2.57 MPa and 10%, respectively. However, the temperature change cannot be detected at the monitoring well. Therefore, a designed period of 3 years for injection test is enough for capturing the main behavior of CO_2 injected into the depleted gas reservoir.

Figure 9 shows the spatial distribution of pressure increment. Controlled by the faults, the pressure propagates along the northeast and southwest. After an injection over 3 years, a pressure increment of 1 bar is built up at a distance of 10 km away from the injection well and at a distance of 18 km after 10 years' injection. Figure 10 shows that the injected CO_2 displaces natural gas in the reservoir and three zones, the CO_2-dominant zone and the zone of CO_2/CH_4 mixture as well as the CH_4-dominant zone, are formed. The migration distances of CO_2 are about 1.6 km and 5 km in 3 years and 10 years, respectively. They are much shorter than those of pressure propagation. It is observed in Figure 11 that the zone of temperature change is very small stretching 1-2 km away from the injection well. In this zone, the temperature gradually decreases outwards from 80°C to 33°C. The

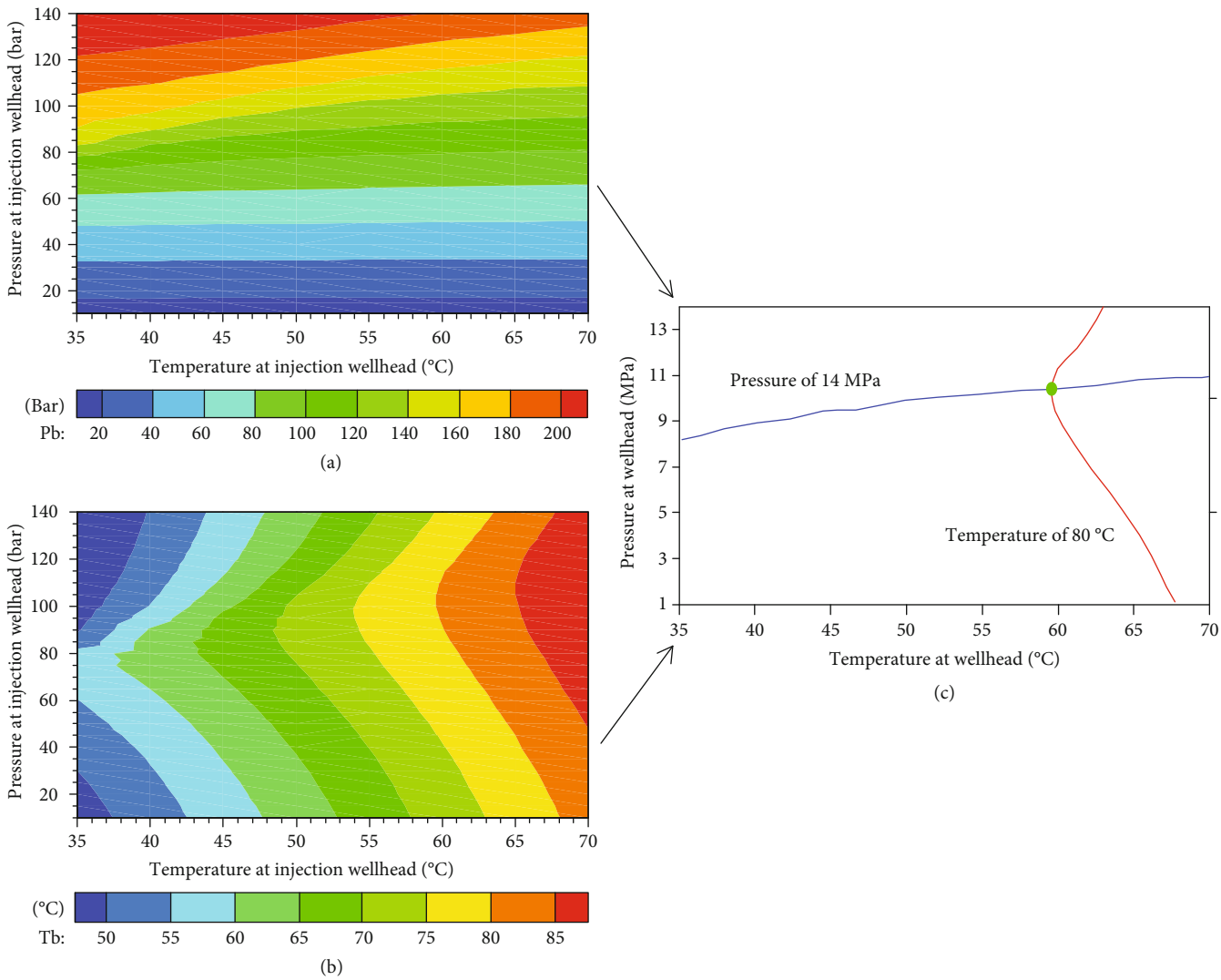

Figure 12: Calculated downhole pressure (a) and temperature (b) to determine the wellhead operation parameters (c).

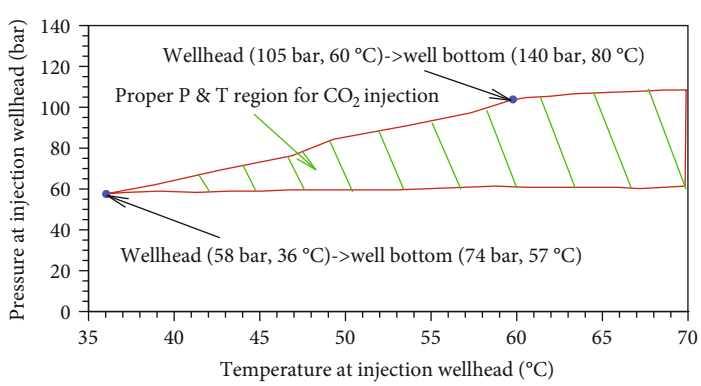

Figure 13: The zone of pressure and temperature allowable for CO_2 injection.

zone showing temperature decrease first extends and then shrinks due to the fact that the Joule-Thomson effect exerts dominantly at the early stage of injection and is alleviated when the pressure in the well increases with time and the fact that the injected CO_2 of high temperature would heat the reservoir rock.

4.2. Wellbore. The state of flow in the wellbore experiences two sequential stages during CO_2 injection: the transient flow stage and the quasi-steady-state flow stage. At the transient flow stage, the injected CO_2 displaces CH_4 and the formation water inducing a dramatically varying flow rate. Due to further injection, CO_2 enters the formation and gradually

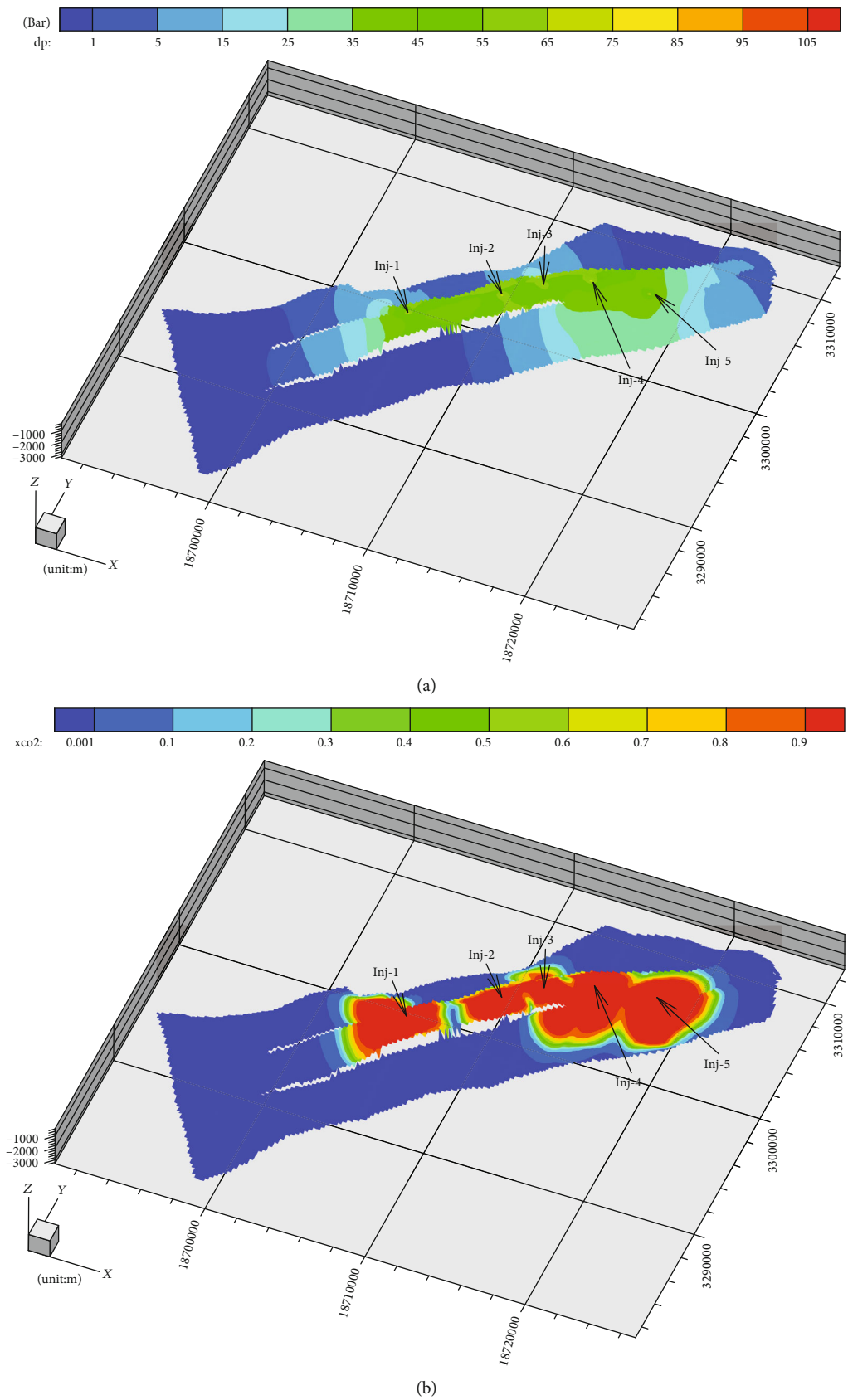

Figure 14: Distribution of pressure increment and CO_2 mass fraction in the gas phase after multiwell injection of 10 years.

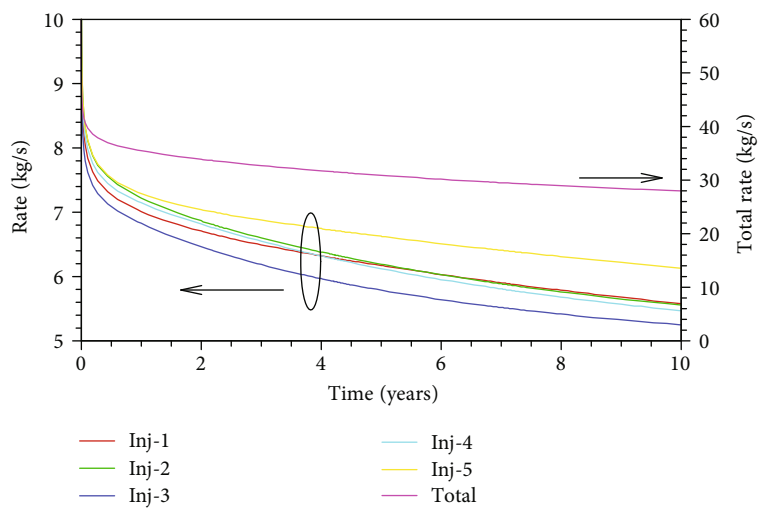

Figure 15: Variation of injection rate with time for multiwell injection.

reaches the quasi-steady state resulting in concomitantly stabilized pressure and flow rate in the wellbore. Compared with the quasi-steady-state flow stage, the transient flow stage is very short and, accordingly, neglected in the present study. Without considering the effect of wellbore friction, the pressure gradient is only attributed to gravity being formulated as $\Delta P = \rho_{CO_2} g \Delta z$ [33], where the density of CO_2 is pressure- and temperature-dependent. The enthalpy of CO_2 along the wellbore is calculated as $\Delta H = g\Delta z$ [33] ignoring the heat transfer between CO_2 and the wall rock in the wellbore. The calculation of pressure, enthalpy, and temperature in the wellbore follows the method as presented by Pruess [34]. When the length of the wellbore L is evenly divided into N levels of a unit length $\Delta z = L/N$, the pressure P_{n+1} at the level of $(n+1)\Delta z$ is calculated recursively based on the pressure P_n at the upper level of $n\Delta z$ as $P_{n+1} = P_n + \rho_n \Delta z$. Similarly, the enthalpy at the corresponding level is calculated by assigning $H_{n+1} = H_n + g\Delta z$ and the temperature is derived as $T_{n+1} = T(P_{n+1}, H_{n+1})$, while the values of density and enthalpy of CO_2 are obtained from NIST Chemistry Web Book [35].

The downhole temperature and pressure calculated based on the wellhead pressure and temperature are presented in Figures 12(a) and 12(b), respectively. Corresponding to the downhole pressure of 14 MPa and temperature of 80°C for maximizing the injection rate (see Section 4.1), the wellhead pressure and temperature should be 10.5 MPa and 60°C, respectively. The zone of pressure and temperature allowable for CO_2 injection corresponding to Figure 6 is shown in Figure 13.

5. Discussions

5.1. Multiwell Injection. A commercially scaled (megaton/a) CO_2 injection project needs at least 4 more wells when the single-well injectivity (20×10^4 tons/a) is taken into account. The potential wells that can be used for CO_2 injection, including Cao 9 (Inj-1), Cao 30 (Inj-2), Cao 31 (Inj-3), Cao 6 (Inj-4), and Cao 22 (Inj-5), are employed in the multiwell injection strategy. The spatial distributions of pressure increment and CO_2 mass fraction in the gas after an injection over 10 years are, respectively, presented in Figure 14. As observed, the pressure increment of 1 bar almost arrives at the northeastern boundary and the CH_4 accumulates between the adjacent wells due to the CO_2 displacement. As illustrated in Figure 15, the total injection rate decreases from 35 kg/s in the first year to 28 kg/s in the 10th year, and the well Cao 22 (Inj-5) shows the highest injection rate among the five as the pressure gradient in the vicinity of this well is relatively higher allowing for easier propagation of CO_2 apart from the well.

5.2. Effect of Permeability. In order to investigate the effect of permeability on CO_2 injection, we simulate the spatial distributions of pressure increment and CO_2 mass fraction in the gas phase, respectively, for the permeability of 0.7 mD and 50 mD as shown in Figure 16. In the case of low permeability, the domain approached by CO_2 is very small due to the low injection rate of 0.79 kg/s (Figure 17). In the case of high permeability, the pressure increment of 1 bar is nearly built up at the boundary of the reservoir (Figure 16(c)) due to the high injection rate of 42.8 kg/s (Figure 17), and almost half of the reservoir is filled by the injected CO_2 (Figure 16(d)). In addition, the injection rates show approximately linear dependence on permeability.

5.3. Effect of Depleted Pressure. The depleted pressure in the reservoir has important effect on the injection pressure and temperature. Generally, both of the injection pressure and temperature decrease with increasing depleted pressure. When the depleted pressure increases from 2 MPa to 6 MPa, the required downhole temperature decreases from 80°C to 50°C presenting a faster reduction rate at higher magnitudes of the depleted pressure (Figure 18). There are two reasons for this observation: (1) a decrease in pressure gradient near the injection well with an increased depleted pressure and (2) a reduction in the Joule-Thomson coefficient with

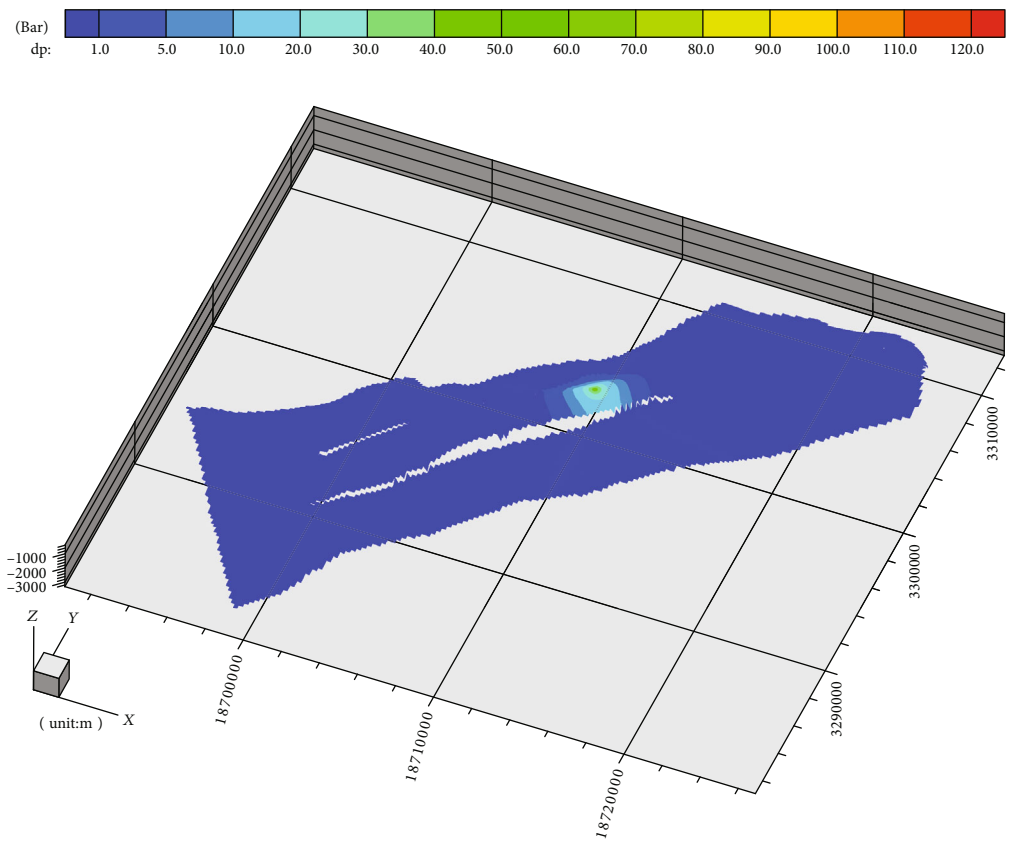

(a)

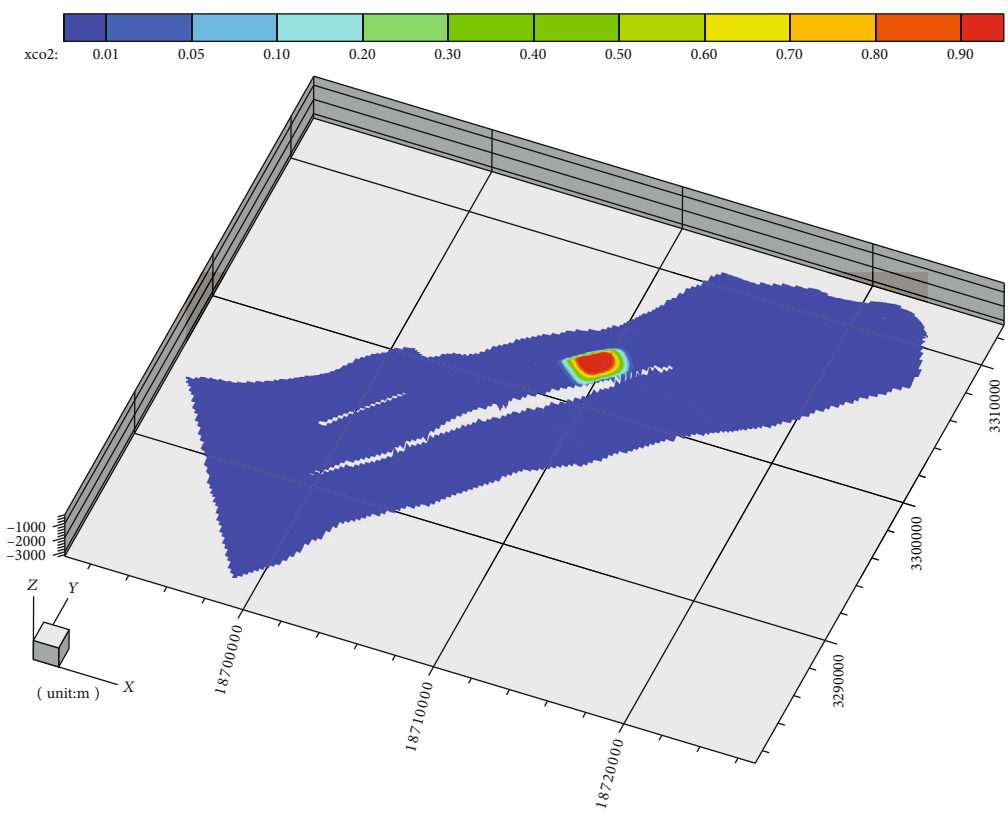

(b)

Figure 16: Continued.

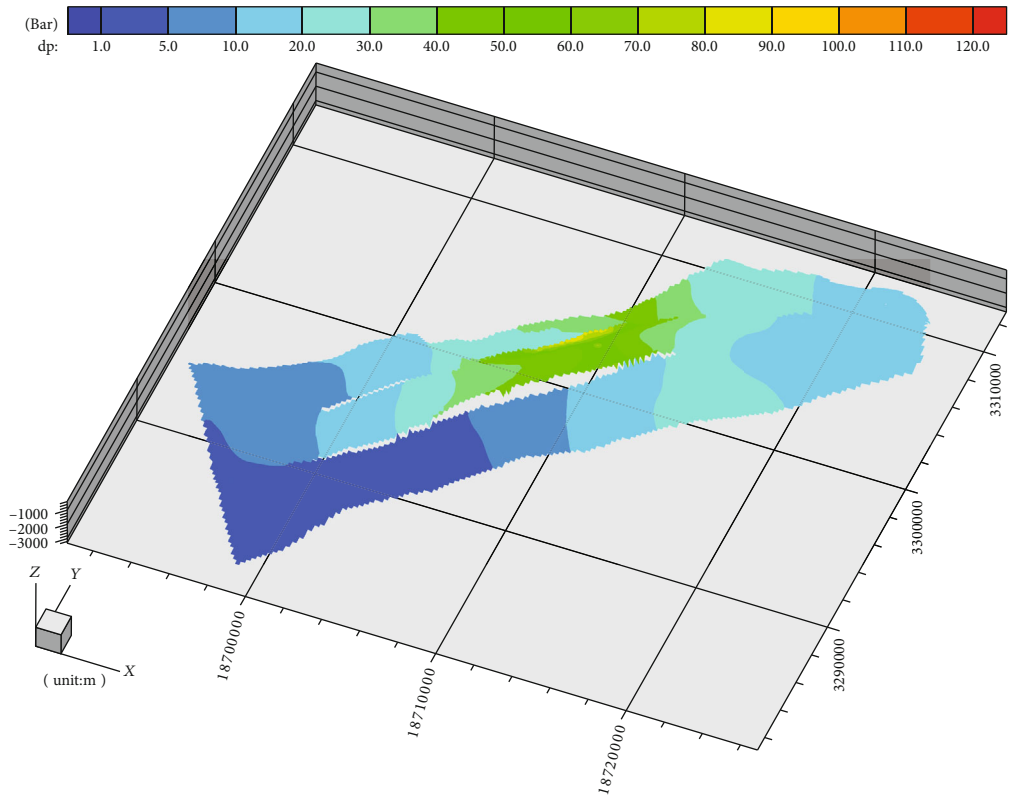

(c)

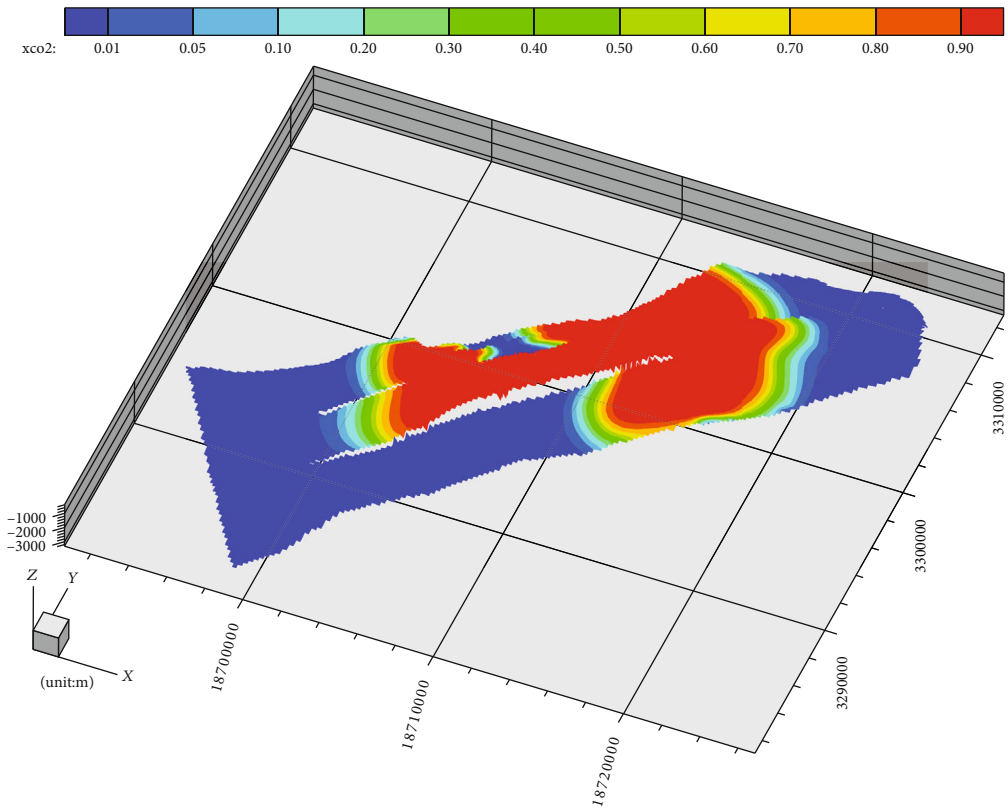

(d)

Figure 16: Effect of permeability on distributions of pressure increment and CO_2 mass fraction in the gas phase.

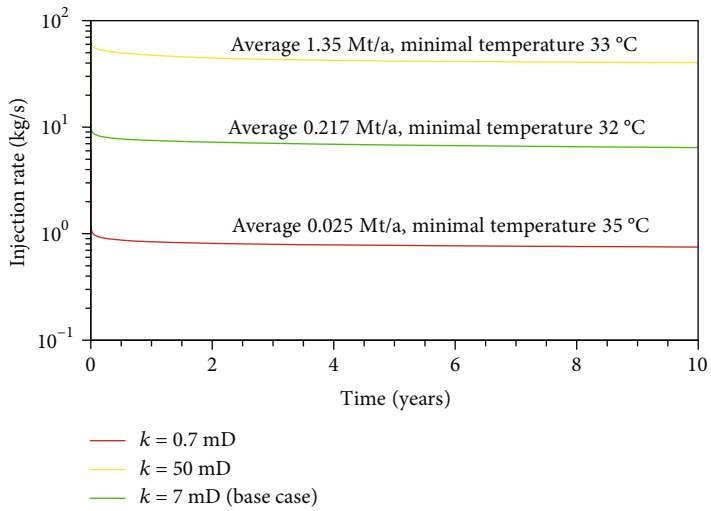

Figure 17: Variation of injection rate with time in the cases of differing permeability.

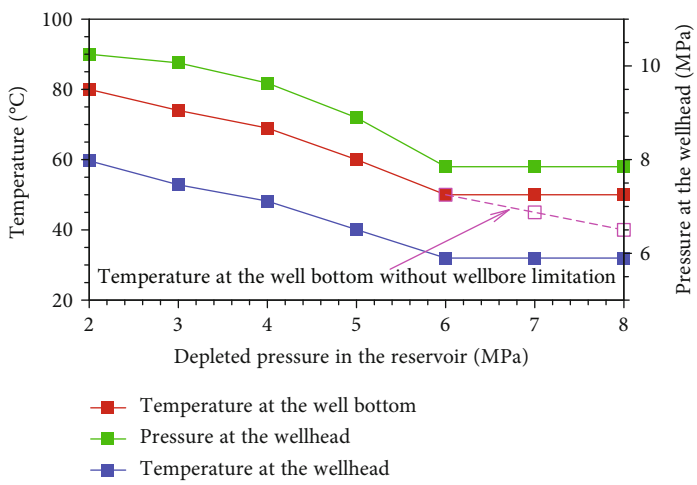

Figure 18: Effect of depleted pressures on injection pressure and temperature.

increasing pressure. In addition, the corresponding wellhead temperature decreases from 60°C to 32°C (Figure 18) leading to an increase in density and, ultimately, a reduction in the required wellhead pressure. Moreover, it is noted that the wellhead temperature decreases below 32°C, when the depleted pressure is higher than 6 MPa, which may induce unexpected phase change of CO_2 in the wellbore. Not least, the injection rate seems not to be obviously affected by the depleted pressure below 6 MPa, however, decreasing significantly due to a diminished pressure gradient when the depleted pressure is above 6 MPa (Figure 19).

5.4. Combination of CO_2 Storage with Enhanced Gas Recovery. CO_2-EGR not only partly offsets the cost of CO_2 storage but also manages the pressure in the reservoir keeping optimized injectivity of CO_2. We therefore evaluate the injection rate of CO_2 as well as the production rate of CH_4 via simulating a combined injection strategy aiming at CO_2-EGR. First, the well Cao 30 (Inj-2) is used for CO_2 injection while the other wells (Inj-1, Inj-3 to Inj-5; see Section 5.1) are used for CH_4 production at a constant production pressure. When CO_2 arrives at the wells for CH_4 production sequentially, these wells are then switched from CH_4 production to CO_2 injection. Figure 20 illustrates the evolution of production rate and injection rate of respective well showing that the production time is 2.0 years, 5.0 years, and 8.4 years for Cao 31 (Inj-3), Cao 6 (Inj-4), and Cao 22 (Inj-5), respectively. By the combined injection and production strategy, the average injection rate amounts to 6.60 kg/s, being higher than the injection rate of 6.28 kg/s by the multiwell injection strategy (see Section 4.1), and the so induced production rate ranges from 0.0 to 0.09 kg/s delivering a cumulative gas production of 1.58×10^7 kg. Moreover, as shown in Figure 21, there is no CH_4 retention between any two wells due to simultaneous CO_2 injection as observed in the case of multiwell injection.

6. Summary and Conclusions

The Sichuan Basin has a large capacity for CO_2 storage in depleted gas reservoirs. The Huangcaoxia gas field, which is nearly depleted and of relatively large storage capacity, is

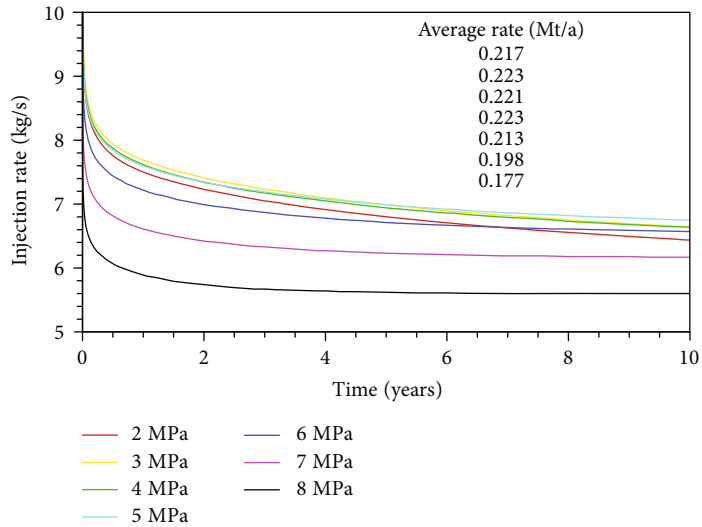

Figure 19: Effect of depleted pressures on injection rate.

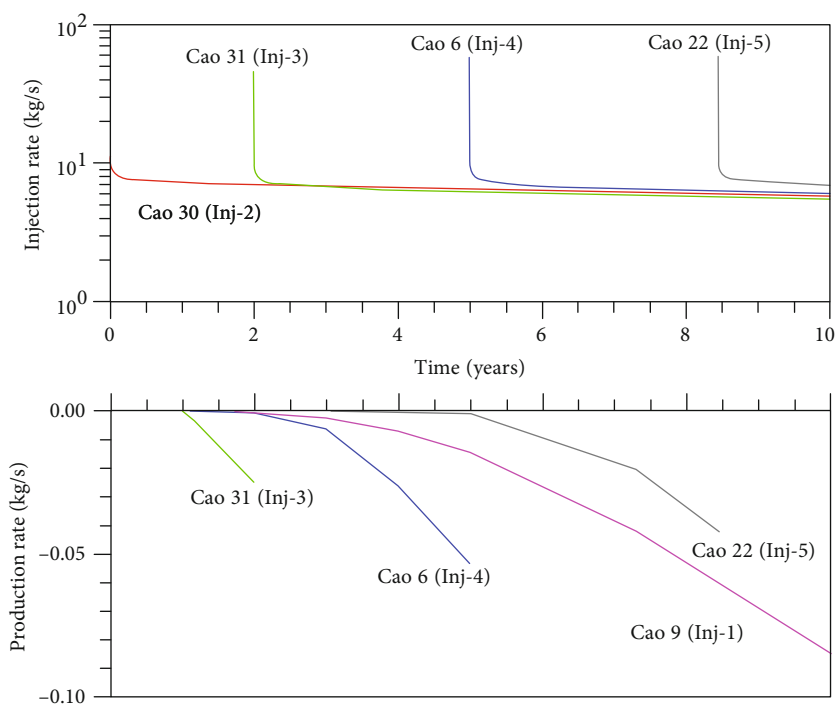

Figure 20: Variation of production and injection rates for CO_2-EGR.

the most advantageous site for a pilot project of CO_2 injection and storage in the eastern Sichuan Basin. Based on the geological and hydrogeological conditions in the Huangcaoxia gas field, a coupled thermal-hydrodynamic model is employed to evaluate the feasibility of CO_2 injection. Major findings and conclusions from our simulations are summarized as follows:

(1) In the well Cao 30, chosen as an injection well, the downhole temperature should be at least 80°C at the downhole pressure of 14 MPa for offsetting the temperature drop in the reservoir due to the strong Joule-Thomson effect. The corresponding injection pressure and temperature at the wellhead are 10.5 MPa and 60°C, respectively, as derived from a simple analytical model

(2) As the reservoir is confined by the faults striking northeast, the injected CO_2 migrates in the reservoir, thereby, along the fault strike. The injected CO_2 arrives at the monitoring well Cao 31, over a distance of 2600 m from the injection well, after an injection over 2 years, while the distances traveled by the pressure buildup and by the CO_2 plume after an injection

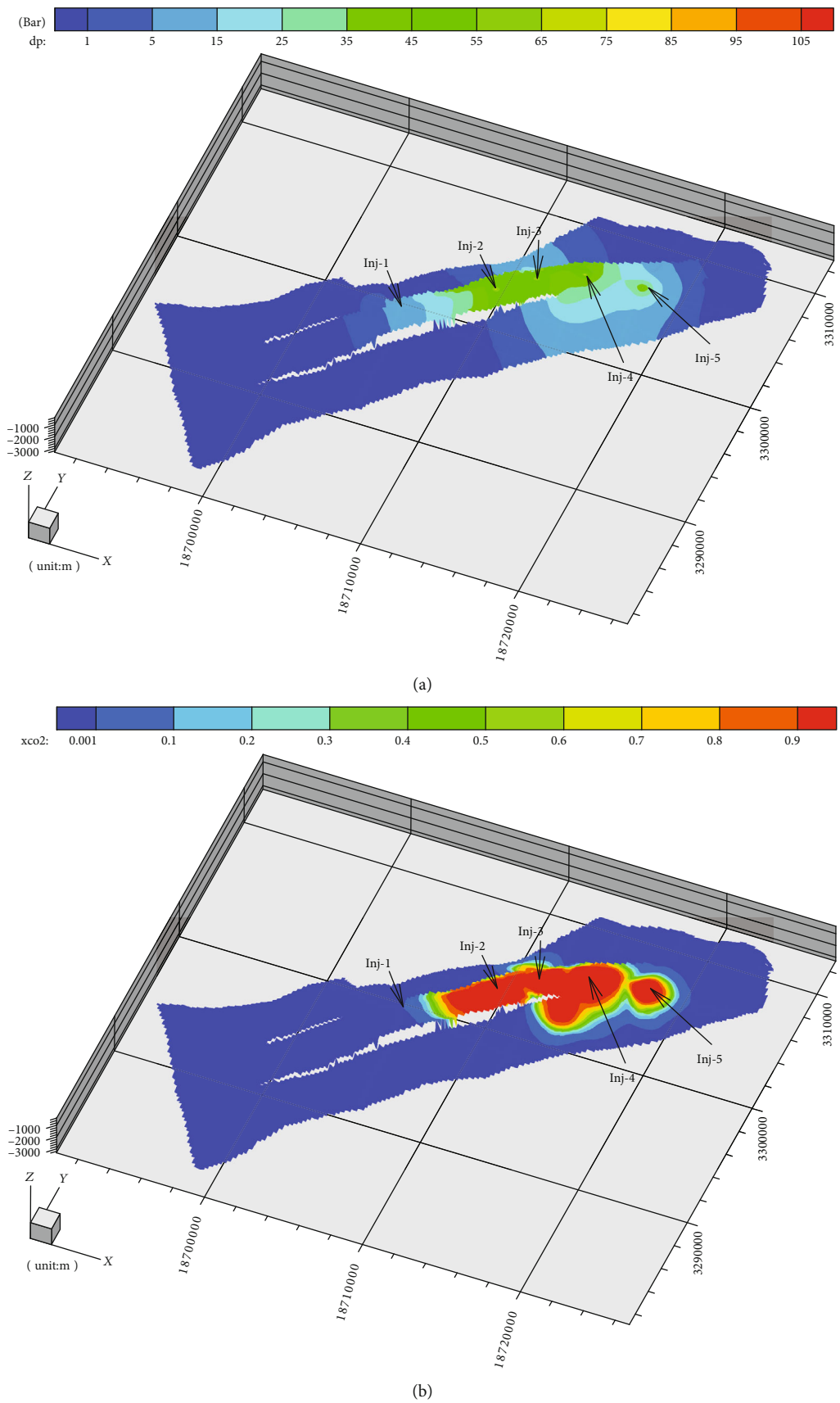

Figure 21: Spatial distribution of pressure increment (a) and CO_2 mass fraction (b) for CO_2-EGR in 10 years.

over 10 years are 18 km and 5 km, respectively. The zone with temperature change is very small being about 1-2 km away from the injection well. The injection rate of the well Cao 31 averages 6.89 kg/s (21.73×10^4 tons/a)

(3) For a large-scale CO_2 injection, the five existing wells (Cao 9, Cao 30, Cao 31, Cao 6, and Cao 22) can be employed simultaneously delivering a total injection rate of 35 kg/s (110×10^4 tons/a). The permeability in the reservoir should be carefully evaluated due to its critical effect on the injectivity

(4) When the depleted pressure is below 6 MPa, both of the injection pressure and temperature decrease with increasing depleted pressure. However, the effect of the depleted pressure on the injection rate is not obvious

(5) The application of CO_2-enhanced gas recovery (CO_2-EGR) can manage the pressure in the reservoir and keep optimized injectivity of CO_2. The optimized injection rate averages 6.60 kg/s, higher than the rate of 6.28 kg/s as delivered by the multiwell injection strategy. The corresponding production rate of natural gas ranges from 0.0 to 0.09 kg/s producing a cumulative gas production of 1.58×10^7 kg over 10 years

Although the numerical simulation provides a detailed view on the feasibility of CO_2 storage in the nearly depleted Huangcaoxia gas field, there are still uncertainties related to the unknown details of the reservoir conditions such as the distribution of reservoir thickness and permeability, the boundary conditions, the effects of formation water, and the water-rock-gas interactions. The model should therefore be updated by taking into consideration the aforementioned uncertainties, and its reliability and accuracy also need to be verified and calibrated by injection tests, which will be the focus of future study within this context.

Data Availability

The data used to support the findings of this study are included within the article.

Conflicts of Interest

The authors declare that there are no conflicts of interest regarding the publication of this paper.

Authors' Contributions

H.L. carried out the simulations, performed data analysis, and wrote the draft manuscript. Q.Z. provided the geological data and performed the preliminary results of the study area. X.L. provided some thoughts and discussed with H.L. and Q.Z.

Acknowledgments

This work was jointly supported by the National Natural Science Foundation of China (Grant Nos. 41602255 and 41672252) and the China Prosperity Fund (CPF) supported by UK government.

References

[1] IPCC, *Special Report on Carbon Dioxide Capture and Storage*, Cambridge University Press, Cambridge, UK, and New York, NY, USA, 2005.

[2] M. D. Aminu, S. A. Nabavi, C. A. Rochelle, and V. Manovic, "A review of developments in carbon dioxide storage," *Applied Energy*, vol. 208, pp. 1389–1419, 2017.

[3] B. van der Meer, "Carbon dioxide storage in natural gas Reservoir," *Oil & Gas Science and Technology - Rev. IFP*, vol. 60, no. 3, pp. 527–536, 2005.

[4] IEA, *CO2 storage in depleted gas fields*, IEA Greenhouse Gas R&D Programme, 2009.

[5] V. Vandeweijer, B. van der Meer, C. Hofstee, F. Mulders, D. D'Hoore, and H. Graven, "Monitoring the CO_2 injection site: K12-B," *Energy Procedia*, vol. 4, pp. 5471–5478, 2011.

[6] J. Monne and C. Prinet, "Lacq-Rousse industrial CCS reference project: description and operational feedback after two and half years of operation," *Energy Procedia*, vol. 37, pp. 6444–6457, 2013.

[7] C. Prinet, S. Thibeau, M. Lescanne, and J. Monne, "Lacq-Rousse CO2 capture and storage demonstration pilot: lessons learnt from two and a half years monitoring," *Energy Procedia*, vol. 37, pp. 3610–3620, 2013.

[8] CLEAN Partners, M. Kühn, M. Tesmer et al., "CLEAN: project overview on CO2 large-scale enhanced gas recovery in the Altmark natural gas field (Germany)," *Environmental Earth Sciences*, vol. 67, no. 2, pp. 311–321, 2012.

[9] J. Underschultz, C. Boreham, T. Dance et al., "CO2 storage in a depleted gas field: an overview of the CO2CRC Otway Project and initial results," *International Journal of Greenhouse Gas Control*, vol. 5, no. 4, pp. 922–932, 2011.

[10] C. R. Jenkins, P. J. Cook, J. Ennis-King et al., "Safe storage and effective monitoring of CO2 in depleted gas fields," *Proceedings of the National Academy of Sciences of the United States of America*, vol. 109, no. 2, pp. E35–E41, 2012.

[11] C. M. Oldenburg, K. Pruess, and S. M. Benson, "Process modeling of CO2Injection into natural gas reservoirs for carbon sequestration and enhanced gas recovery," *Energy & Fuels*, vol. 15, no. 2, pp. 293–298, 2001.

[12] C. M. Oldenburg, S. H. Stevens, and S. M. Benson, "Economic feasibility of carbon sequestration with enhanced gas recovery (CSEGR)," *Energy*, vol. 29, no. 9-10, pp. 1413–1422, 2004.

[13] C. M. Oldenburg, G. J. Moridis, N. Spycher, and K. Pruess, "EOS7C version 1.0: TOUGH2 module for carbon dioxide or nitrogen in natural gas (methane) reservoirs," in *Earth Science Division*, Lawrence Berkeley National Laboratory, University of California, Berkeley, 2004.

[14] J. Ennis-King, T. Dance, J. Xu et al., "The role of heterogeneity in CO_2 storage in a depleted gas field: history matching of simulation models to field data for the CO2CRC Otway Project, Australia," *Energy Procedia*, vol. 4, pp. 3494–3501, 2011.

[15] S. Thibeau, P. Chiquet, C. Prinet, and M. Lescanne, "Lacq-Rousse CO_2 Capture and Storage Demonstration Pilot: Lessons

Learnt from Reservoir Modelling Studies," *Energy Procedia*, vol. 37, pp. 6306–6316, 2013.

[16] Y. Gou, Z. Hou, H. Liu, L. Zhou, and P. Were, "Numerical simulation of carbon dioxide injection for enhanced gas recovery (CO2-EGR) in Altmark natural gas field," *Acta Geotechnica*, vol. 9, no. 1, pp. 49–58, 2014.

[17] C. M. Oldenburg, "Joule-Thomson cooling due to CO_2 injection into natural gas reservoirs," *Energy Conversion and Management*, vol. 48, no. 6, pp. 1808–1815, 2007.

[18] F. Luo, R. N. Xu, and P. X. Jiang, "Numerical investigation of the influence of vertical permeability heterogeneity in stratified formation and of injection/production well perforation placement on CO_2 geological storage with enhanced CH_4 recovery," *Applied Energy*, vol. 102, pp. 1314–1323, 2013.

[19] M. J. Patel, E. F. May, and M. L. Johns, "High-fidelity reservoir simulations of enhanced gas recovery with supercritical CO_2," *Energy*, vol. 111, pp. 548–559, 2016.

[20] Y. S. Ma, X. Y. Cai, P. R. Zha, Y. Luo, and X. F. Zhang, "Distribution and further exploration of the large-medium sized gas fields in Sichuan Basin," *Acta Petrolei Sinica*, vol. 31, no. 3, pp. 347–354, 2010.

[21] Y. Liu, X. C. Li, Z. M. Fang, and B. Bai, "Preliminary estimation of CO2 storage capacity in gas field in China," *Yantu Lixue(Rock and Soil Mechanics)*, vol. 27, no. 12, pp. 2276–2281, 2006.

[22] Y. Diao, G. Zhu, H. Cao, C. Zhang, X. Li, and X. Jin, "Mesoscale assessment of CO2 storage potential and geological suitability for target area selection in the Sichuan Basin," *Geofluids*, vol. 2017, Article ID 9587872, 17 pages, 2017.

[23] S. Bachu and J. Shaw, "Evaluation of the CO sequestration capacity in Alberta's oil and gas reservoirs at depletion and the effect of underlying aquifers," *Journal of Canadian Petroleum Technology*, vol. 42, no. 09, pp. 51–61, 2003.

[24] M. T. Reagan and C. M. Oldenburg, *WebGasEOS v1. 0 user guide. Lawrence Berkeley National Laboratory Report (Vol. 3188)*, 2006.

[25] K. Pruess and J. Garcia, "Multiphase flow dynamics during CO_2 disposal into saline aquifers," *Environmental Geology*, vol. 42, no. 2-3, pp. 282–295, 2002.

[26] S. J. Zarrouk and T. A. Moore, "Preliminary reservoir model of enhanced coalbed methane (ECBM) in a subbituminous coal seam, Huntly Coalfield, New Zealand," *International Journal of Coal Geology*, vol. 77, no. 1-2, pp. 153–161, 2009.

[27] H. Lei, J. Li, X. Li, and Z. Jiang, "EOS7Cm: an improved TOUGH2 module for simulating non-isothermal multiphase and multicomponent flow in CO_2-H_2S-CH_4-brine systems with high pressure, temperature and salinity," *Computers & Geosciences*, vol. 94, pp. 150–161, 2016.

[28] H. Lei, J. Li, X. Li, and Z. Jiang, "Numerical modeling of co-injection of N_2 and O_2 with CO_2 into aquifers at the Tongliao CCS site," *International Journal of Greenhouse Gas Control*, vol. 54, pp. 228–241, 2016.

[29] M. T. van Genuchten, "A closed-form equation for predicting the hydraulic conductivity of unsaturated Soils," *Soil Science Society of America Journal*, vol. 44, no. 5, pp. 892–898, 1980.

[30] A. T. Corey, "The interrelation between gas and oil relative permeability," *Producers Monthly*, vol. 19, no. 1, pp. 38–41, 1954.

[31] "Calsep.PVTSim, Version 10," 1997, http://www.Calsep.com.

[32] C. M. Oldenburg and S. M. Benson, *Carbon sequestration with enhanced gas recovery: identifying candidate sites for pilot study (No. LBNL-47580)*, Lawrence Berkeley National Lab.(LBNL), Berkeley, CA (United States), 2001.

[33] A. D. Atrens, H. Gurgenci, and V. Rudolph, "Electricity generation using a carbon-dioxide thermosiphon," *Geothermics*, vol. 39, no. 2, pp. 161–169, 2010.

[34] K. Pruess, "Enhanced geothermal systems (EGS) using CO_2 as working fluid–A novel approach for generating renewable energy with simultaneous sequestration of carbon," *Geothermics*, vol. 35, no. 4, pp. 351–367, 2006.

[35] NIST (National Institute of Science and Technology), "NIST Chemistry WebBook: NIST Standard Reference Database Number 69," http://webbook.nist.gov/chemistry/.